LAYER-BY-LAYER DEPOSITION OF TANNIC ACID AND POLY(2-ISOPROPYL-2-OXAZOLINE) ONTO IRON OXIDE NANOPARTICLES

A THESIS SUBMITTED TO
THE GRADUATE SCHOOL OF NATURAL AND APPLIED SCIENCES
OF
MIDDLE EAST TECHNICAL UNIVERSITY

BY

MAJID AKBAR

IN PARTIAL FULFILLMENT OF THE REQUIREMENTS
FOR
THE DEGREE OF MASTER OF SCIENCE
IN
POLYMER SCIENCE & TECHNOLOGY

SEPTEMBER 2017

Approval of the thesis:

LAYER-BY-LAYER DEPOSITION OF TANNIC ACID AND POLY(2-ISOPROPYL-2-OXAZOLINE) ONTO IRON OXIDE NANOPARTICLES

submitted by **MAJID AKBAR** in partial fulfillment of the requirements for the degree **of Master of Science in Polymer Science & Technology Department, Middle East Technical University** by,

Prof. Dr. Mevlüde Gülbin Dural Ünver _____
Dean, Graduate School of **Natural and Applied Sciences**

Prof. Dr. Necati Özkan _____
Head of Department, **Polymer Science & Technology**

Assoc. Prof. Dr. Irem Erel Göktepe _____
Supervisor, **Polymer Science & Technology, METU**

Examining Committee Members:

Prof. Dr. Ali Çırpan _____
Chemistry Dept., METU

Assoc. Prof. Dr. Irem Erel Göktepe _____
Chemistry Dept., METU

Assoc.Prof. Dr. Gülay Ertaş _____
Chemistry Dept., METU

Assoc. Prof. Dr. Emren Esentürk _____
Chemistry Dept., METU

Assoc. Prof. Dr. Pınar Yılgör Huri _____
Biomedical Engineering Dept., Ankara University

Date:

I hereby declare that all information in this document has been obtained and presented in accordance with academic rules and ethical conduct. I also declare that, as required by these rules and conduct, I have fully cited and referenced all material and results that are not original to this work.

Name, Last name: **MAJID AKBAR**

Signature:

ABSTRACT

LAYER-BY-LAYER DEPOSITION OF TANNIC ACID AND POLY(2-ISOPROPYL-2-OXAZOLINE) ONTO IRON OXIDE NANOPARTICLES

AKBAR, Majid
M.Sc., Department of Polymer Science and Technology
Supervisor: Assoc. Prof. Dr. Irem Erel Göktepe

September 2017, 80 pages

Layer-by-layer (LbL) technique is a simple and unique technique for fabrication of thin films. It is possible to control the film properties during assembly and post-assembly steps. Stimuli responsive polymers are important building blocks for LbL assembly, especially for drug delivery applications of LbL films. Iron oxide nanoparticles have been of interest for biomedical applications such as bioimaging and/or drug delivery via magnetothermal trigger.

This thesis study aimed to develop strategies for layer-by-layer assembly of neutral polymers onto iron oxide nano particles. Iron oxide nano particles were synthesized by ultrasound based co-precipitation method and characterized by dynamic light scattering, FTIR spectroscopy and transmission electron microscopy techniques. Multilayers of poly(2-isopropyl-2-oxazoline) (PIPOX) and Tannic Acid (TA) were deposited onto iron oxide nano particles using LbL technique. The driving force for multilayer assembly was found to be hydrogen bonding interactions among PIPOX and TA. Film deposition onto iron oxide nanoparticles was characterized using zeta potential and hydrodynamic size measurements.

A model anti-cancer drug, doxorubicin (DOX) was loaded into LbL coated iron oxide nanoparticles at pH 7.5. It was shown that DOX could be released from the surface of LbL coated iron oxide nanoparticles via both pH and temperature-trigger. DOX released from the surface at moderately acidic conditions due to protonation of TA and loss in electrostatic interactions among TA and DOX. On the other hand, DOX was released from the surface via temperature-trigger due to lower critical solution temperature (LCST)-type phase behavior of PIPOX and conformational transition in PIPOX chains within the multilayers resulting in release of DOX molecules.

Considering the temperature and pH response of multilayer and potential of iron oxide nanoparticles for biomedical applications, results obtained in this thesis are important to develop strategies for LbL coating of iron oxide nanoparticles and release of drug molecules from surfaces.

Keywords: Layer-by-layer, stimuli responsive, iron oxide nanoparticles, poly(2-isopropyl-2-oxazoline)

ÖZ

TANİK ASİT VE POLİ(2-İZOPROPİL-2OKSAZOLİN)'İN DEMİR OKSİT NANOPARÇACIKLARI ÜZERİNE KATMAN-KATMAN KENDİLİĞİNDEN YAPILANMASI

AKBAR, Majid
Yüksek Lisans, Polimer Bilim ve Teknolojisi
Tez yöneticisi: Doç. Dr. Irem Erel Göktepe

Eylül 2017, 80 sayfa

Katman-katman (LbL) kendiliğinden yapılanma yöntemi ince filmlerin hazırlanmasında kullanılan basit ve yenilikçi bir yöntemdir. Film özelliklerinin kontrolü gerek film üretimi gerek ise film üretimi sonrasında mümkündür. Uyarıcılara duyarlı polimerler, özellikle biyomedikal uygulamalarda kullanılacak LbL filmlerin hazırlanmasında önemli yapıtaşlarıdır. Demir oksit nanoparçacıkları biyogörüntüleme ve/veya manyetotermal tetikleme ile kontrollü ilaç salımı gibi biyomedikal uygulamalar için ilgi çekmektedir.

Bu tez çalışması LbL yöntemi ile nötr polimerlerin demir oksit nanoparçacıkları yüzeyinde biriktirilmesi için stratejiler geliştirmeyi amaçlamıştır. Demir oksit nanoparçacıkları ultrasound temelli birlikte-çöktürme tekniği ile sentezlenmiş ve dinamik ışık saçılımı, Fourier Dönüşümlü Kızılötesi spektroskopisi ve geçirimli elektron mikroskobu teknikleri kullanılarak tanımlanmıştır. Poly(2-izopropil-2-oksazolin) (PIPOX) and Tanik Asit (TA) demir oksit nanoparçacıkları üzerinde LbL tekniği kullanılarak biriktirilmiştir. Çok-katmanlı filmlerin oluşumu için itici güç PIPOX ve TA arasında oluşan hidrojen bağlarıdır. Demir oksit nanoparçacıkları üzerinde film birikimi zeta potansiyel ve hidrodinamik boyut ölçümleri ile tanımlanmıştır.

Doxorubicin (DOX), model anti-kanser ilacı olarak kullanılmış ve LbL kaplanmış demir oksit nanoparçaçıklarına pH 7.5'de yüklenmiştir. DOX'un LbL kaplı demir oksit nanoparçacıklarının yüzeyinden hem pH hem de sıcaklık tetiklemesi ile salınabileceği gösterilmiştir. DOX'un orta asidik koşullarda salımı, TA'nın protonlanması ve TA ile DOX arasındaki elektrostatik etkileşimin yitirilmesidir. DOX'un yüzeyden sıcaklık tetiklemesi ile salımı ise PIPOX'un alt kritik çözelti sıcaklığı (LCST) tipi faz davranışı göstermesi ve PIPOX'un film içerisinde konformasyonal dönüşüme uğraması sayesinde DOX moleküllerinin salımı ile ilişkilendirilebilir.

Çok-katmanlı filmlerin sıcaklık ve pH duyarlı olması ve demir oksit nanoparçacıklarının biyomedikal uygulamalar için potansiyeli düşünüldüğünde, bu çalışmadan elde edilen sonuçlar demir oksit nanoparçacıkların LbL filmler ile kaplanması ve yüzeylerinden ilaç salımı için stratejiler geliştirilmesine katkısından dolayı önemlidir.

Anahtar kelimeler: katman-katman kendiliğinden yapılanma tekniği, demir oksit nanoparçacıkları, uyarıcılara cevap veren, poli(2-izopropil-2-oksazolin)

To My Family,

ACKNOWLEDGEMENTS

I would like to express my immense reverence and appreciation to Assoc. Prof. Dr. Irem Erel Göktepe for being an idolatrous example and acute in pedagogy and explaining the subtle details of science in a more meticulous and didactic way for a neophyte like me in order to explore the world of science. Throughout this work, she always believed in me and gave me a pleasant environment for being a maverick and developed a variegated personality. It would have been a hyperbole task without her indefatigable efforts.

I would also like to extent my gratitude to my committee members, Prof. Dr. Ali Çirpan, Assoc. Prof. Dr. Gülay Ertaş. Assoc. Prof. Dr. Emren Esentürk and Assoc. Prof. Dr. Pınar Yılgör Huri for providing their precious knowledge and comments with which I have been able to make my thesis better.

This work was financially supported by The Scientific and Technological Research Council of Turkey, TUBITAK (Grant Number: 113Z586).

I also would like to thank Higher Education Commission (HEC), Pakistan for financially supporting me to complete my studies here.

I am highly obliged to my parents and my family who always believed in me and supported and encouraged me in the path of education and motivated me to complete my thesis and wish my father would have been there to witness my feat.

I am thankful for my lab mates for being there for me especially Bora Onat, Gökçe Çalıs and Sinem Ulusan for being supportive to me and helping me out when needed.

I also thank Dr. Joydev Manna for always being helpful in matter of science and research and being a big brother here in university.

Also, I am extremely thankful to my friends especially Yusuf Samet Aytekin, Ali Ekber Karabag, Ahmad Bashir and and Shaukat Ali Changezi for memorable Friday nights in the department. I am also thankful to Iqtidar Ali Khan for helping me out in my writing.

Finally, I am extremely thankful to have such great friends here in Ankara (YTB Oldies and Pakistani Community in METU) and back in Pakistan who always believed in me and made my stay here pleasant and for halcyon days else with such language and social barrier in earlier days it would have been a different journey. In a nutshell, it was path worth remembering and much to learn.

TABLE OF CONTENTS

LIST OF FIGURES

FIGURES

LIST OF SCHEMATICS

SCHEMATICS

LIST OF ABBREVIATIONS

LbL	Layer-by-Layer
PDMAC	poly(diallyldimethylammonium chloride)
PSS	poly(styrene sulphonate)
PAH	poly(allylamine hydrochloride)
PAA	poly(acrylic acid)
PMAA	poly(methylacrylic acid)
PNIPAM	poly(N-isopropylacrylamide)
LCST	Lower critical solution temperature
UCST	Upper critical solution temperature
PIPOX	poly(2-isopropyl-2-oxazoline)
TA	Tannic Acid
IONP	Iron oxide nanoparticles
DOX	Doxorubicin
POX	poly(2-alkyl-2-oxazoline)
DI	De ionized water
DLS	Dynamic light scattering

CHAPTER 1

INTRODUCTION

1.1 Layer-by-Layer Self-Assembly Technique

Layer-by-layer (LbL) self-assembly technique is a simple and practical technique for fabrication of thin films. It relies on alternating deposition of oppositely charged speices onto a surface by immersing the substrate sequentially into solutions of positively and negatively charged species. The driving force among the oppositely charged species is electrostatic interactions.

LbL self-assembly technique was first introduced in 1966 by R. K. Iler. Multilayers of alumina and silica colloidal particles were deposited onto glass substrate in a LbL fashion [1]. Layer-by-Layer technique was later on adopted to polyelectrolytes by Decher and Hong in 1992 [2]. As described in Figure 1.1, a positively charged substrate is immersed into solution of a polyanion so that 1-layer of polyanion is deployed on the substrate. Then it is rinsed so that the loosely bound polyanion is removed from the surface. The same process is repeated with the polycation. Multilayer assembly is achieved via electrostatic interactions among the oppositely charged polyelectrolytes and charge reversal after each layer deposition [3]. The cycle is repeated till desired number of layers and thickness of films are achieved.

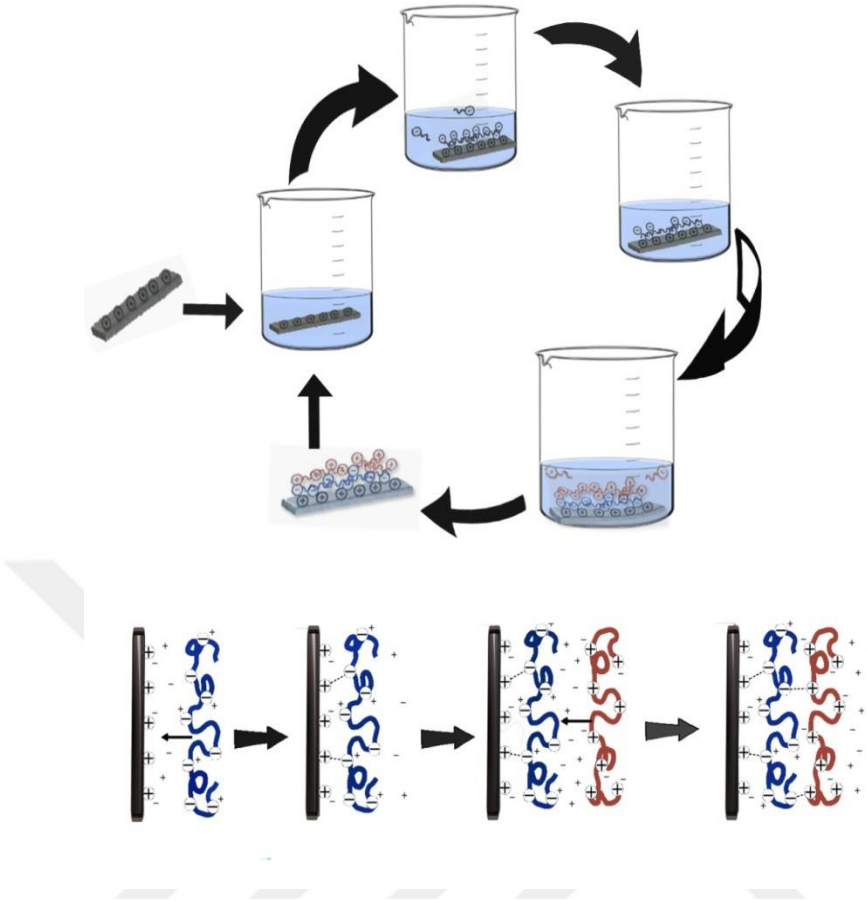

Figure 1.1 Schematic representation of multilayer film preparation via LbL self-assembly technique. Modified from Decher et al. *Science*. 1997 [4].

After this breakthrough and novel discovery of an ultra-thin film preparation technique, intense studies have been performed for practical use of this method specifically in biomedical applications due to possibility of film preparation in aqueous environment. However, the major limitation of electrostatically bound polyelectrolyte multilayers in biomedical applications was the toxic nature of polycations and the multilayers are mostly highly charged and can lead to fouling in biological systems [5]. Thus, efforts were made on introducing neutral polymers into LbL films. The first example of hydrogen-bonded LbL films was demonstrated by Stokton and Rubner in which self-assembly of polyaniline with different neutral polymers (e.g. polyvinylpyrrolidone) at the surface of various substrates such as glass, silicon and plastics was achieved. At the same time, Zhang et al. demonstrated

hydrogen-bonded self-assembly of poly(4-vinylpyridine) and poly(acrylic acid). Hydrogen donor carboxylic groups and hydrogen acceptor pyridine groups drove the multilayer assembly via hydrogen bonding interactions [6]. Later, it was shown that hydrogen-bonded multilayers could be erased from the surface via pH-trigger [7]. Such films were generally composed of hydrogen accepting neutral polymer and a hydrogen donating polyacid and are deposited at the surface at very low pH to assure the protonation of the acid functional groups. By increasing pH, the polyacid component gets ionized, resulting in disruption of hydrogen bonds and removal of the film from the surface. This is the reason why they are called "erasable multilayers" [8].

The most important advantage of fabricating ultra-thin films via LbL technique is the versatility of the polymers that can be used in film preparation. LbL method is not limited to only electrostatic and hydrogen bonding interactions among the layers. Hydrophobic interactions [9], van der Waals forces [10], coordination bonding [11,12] charge-transfer [13], metal-ligand [14–16] and bio-specific [17,18] interactions can also be used as driving forces for multilayer assembly, enabling a wide variety of polymers to be incorporated into LbL films.

LbL technique is advantageous over the other film preparation techniques such as Langmuir Blodgett technique because it is a very simple and economical method [19]. Sophisticated instrumentation is not required for film preparation. A LbL film preparation set-up is composed of beakers and tweezers. There is no substrate limitation for this technique. Glass, quartz, Silicon, Germanium substrates can be used as templates in LbL assembly [19]. LbL technique is environmentally friendly because it allows use of aqueous polymer solutions [20]. Film properties can be finely controlled using this technique. For example, film thickness and morphology can be controlled by assembly and post-assembly conditions [21]. pH, temperature and polymer deposition time play important roles in the growth and properties of multilayers [22] [23].

LbL self-assembly is not restricted only to 2D substrates but can also be applied to 3D substrates [24] such as polystyrene latex [25],metallic nanoparticles[26] [27] and silica particles [28]. In path of taking this technique to 3D substrates, Caruso was the first preparing LbL films on 3D substrates in 1998. In this study, electrostatic multilayers of colloidal silica nanoparticles and poly (diallyldimethylammonium chloride) (PDMAC) were assembled onto polystyrene latex particles as substrates in which the substrates were then removed resulting in hollow polymer capsules [29]. This study opened the gateway towards LbL self-assembly onto 3D substrates and preparation of LbL capsules. Later that year, another try for making multilayer capsules via LbL was done by E.Donath et al. In that study, multilayers of poly(sodium styrenesulphonate) and poly(allylamine hydrochloride) (PAH) were constructed on melamine-formaldehyde colloidal particles [30]. As mentioned earlier, LbL films are promising materials for biomedical applications due to possibility of film preparation in aqueous environment. In this sense, LbL capsules are specifically promising materials for biomedical applications such as drug delivery due to possibility of including and releasing biologically functional molecules within the multilayers [31].

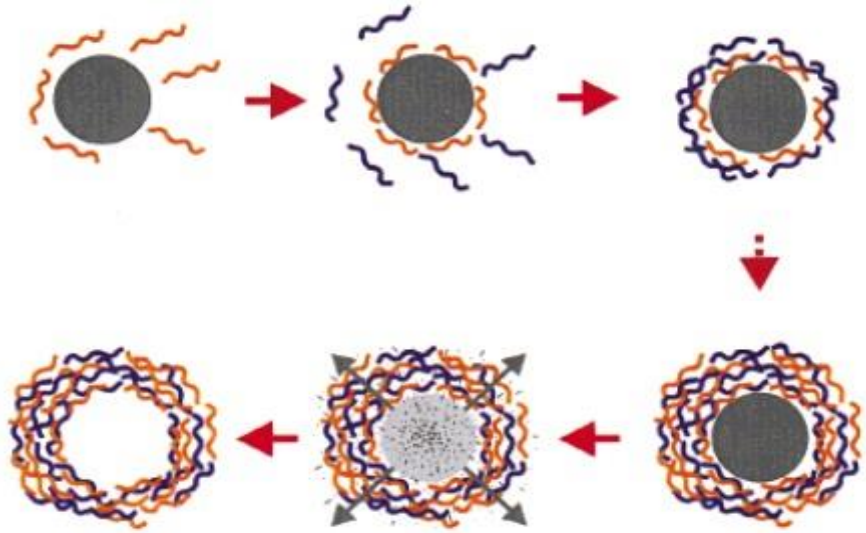

Scheme 1.1 Schematic representation of hollow capsule formation via LbL approach [30]. (Modified from Donath et al. Angew. Chem. Int. Ed. 1998)

1.1.1 Stimuli Responsive Multilayers

Polymers which alter their properties by changing environmental conditions are called "stimuli responsive polymers" or "smart polymers" [32]. The change can be associated with the conformation, solubility and hydrophilic and hydrophobic balance in the structure of the polymer and can be induced via external and/or internal stimuli such as pH, temperature, light, magnetic field and electric field [33]. Among these stimuli, pH and temperature triggers have been extensively studied for drug delivery applications. This is because pH changes at different sites of the body. For example stomach pH varies from 1.0-3.0, colon pH (7.0-7.5), blood pH is in between 7.35-7.45, and duodenum pH varies between 4.8-8.2. Besides, pH can also change at tumor sites which is in between 7.2-6.5 [34,35]. Temperature can also be used as an external trigger in drug delivery applications [36,37].

1.1.1.1 pH-Responsive Multilayers

Weak polyelectrolytes were widely studied for biomedical applications because of their peculiar behavior of being responsive to pH [35]. So a multilayer system composed of weak polyelectrolytes can serve for drug release applications compared to strong polyelectrolytes [38]. Most of the pH-responsive polymers contain acidic and basic pendant groups. For example, poly(acrylic acid) (PAA) and poly(methylacrylic acid) (PMAA) are two polycarboxylic acids which are commonly used in LbL self-assembly and have carboxylic acid pendant groups. Another example is poly(dimethylaminoethyl methacrylate) (PDMAEMA) which is also commonly used in LbL assembly studies has amino pendant groups. The conformation of pH-responsive polymers in aqueous solution change by changing the solution pH [39].

pH-induced release of functional molecules from both electrostatic and hydrogen-bonded multilayers has been demonstrated [38,40]. For example, Sukhishvili reported on release of dyes from hydrogen-bonded multilayers. Hydrogen-bonded multilayers of poly(methylacrylic acid) (PMAA) and poly(ethylene oxide) was constructed at pH 2. Loading of Rhodamine 6G was performed at pH 4.2 when PMAA carried negative charge. Loading was performed via electrostatic interaction among negatively charged PMAA and positively charged Rhodamine 6GRelease of R6G was performed by exposing the film to buffer solution at higher pH when the multilayers are dissolved [41].

G. Sukhorukov et al. reported pH controlled encapsulation of functional molecules from polyelectrolyte capsules. Capsules were fabricated by alternating deposition of poly(styrene sulphonate) (PSS) and poly(allylamine hydrochloride) (PAH) onto melamine formaldehyde template at pH 6.7. Dextran was later loaded in the capsule at pH 3. Dextran release from the multilayers was performed at pH 7. The driving force for Dextran release was the change in the conformation of polymers by altering pH and inducing formation of open and closed capsule walls [42] .

Zhao et al. reported multilayer polyelectrolyte microspheres which were fabricated by LbL assembly of fluorescein isothiocyanate modified chitosan (CSFITC) as the polycation and sodium hyaluronate (HA) as the polyanion. Multilayered assembly was developed on polystyrene sulfonate (PSS) templates with galactosylated chitosan (GC) as the outermost layer. Model drugs as doxorubicin and dipyridamole were encapsulated separately in the multilayered capsule and release studies were examined. Drugs were released at pH 7.4 and 1.8 and pH 7.5 and 5.0 [43].

Lu et al. prepared supramolecular microcapsules for pH controlled drug delivery. Assembly of polyaldehyde dextran-graft-adamantane (PAD-g-AD) and carboxymethyl dextran-graft-β-CD (CMD-g-β-CD) onto $CaCO_3$ particles was performed via LbL technique through host-guest interactions among the layers. Microcapsules were prepared at pH 7.4. In-vivo drug release was studied at pH 5.5 and 7.4. It is observed that at weak acidic conditions, microcapsules were destructed and drug was released [44,45].

Erel et al. reported release of pyrene from multilayers of tannic acid and poly[2-(N-morpholino)ethylmethacrylate-*block*-2-(diisopropylamino)ethylmethacrylate] (PMEMA-*b*-PDPA) micelles. Multilayer assembly was fabricated at pH 7.4. It was observed that when pH is decreased below pK_a of PDPA block, micelles went into disintegration and pyrene was released [46].

1.1.1.2 Temperature-Responsive Multilayers

Temperature-responsive or thermo-responsive polymers change their conformation at a critical temperature [47]. In this respect, polymers are categorized in two parts: 1) polymers exhibiting lower critical solution temperature (LCST) and 2) polymers exhibiting upper critical solution temperature (UCST). Polymer solution which shows the phase separation with increasing temperature, then the polymer has LCST. A polymer which shows similar behavior by decreasing temperature possesses UCST [48]. For biomedical applications, polymers with LCST were more extensively

studied because such polymers are readily soluble in aqueous environment at low temperatures and they are less toxic in nature [49]. The phase separation in polymer solutions with LCST is basically caused by hydrogen bonding breaking among the polymer and water molecules. Therefore, many of the temperature-responsive polymers are neutral polymers and majority of temperature-responsive LbL films are constructed using these neutral polymers. In other words, many of the temperature-responsive LbL films that have been reported in the literature are hydrogen bonding driven systems [50,51].

The most commonly used temperature-responsive polymer that has been used for biomedical applications was poly(N-isopropylacrylamide) (PNIPAM) due to its LCST of 32-34oC which is very close to human body temperature [52,53]. There are many examples of temperature-responsive LbL films in the literature and significant amount of them are based on PNIPAM [52,54–56].

Caruso et al. assembled temperature responsive multi-layer assembly via LbL technique. Multilayers of poly(N-isopropylacrylamide) (PNIPAM) and poly(acrylic acid) (PAA) were assembled at pH 3 on quartz slides so that acrylic acid is protonated and hydrogen bonding can be the driving force of the multilayer assembly. It was shown that the amount adsorbed was higher when PNIPAM adsorption was conducted around LCST of PNIPAM. Multilayers were later impregnated with Rhodamine dye for release studies. The release studies were obtained at 21^{o}C and 50^{o}C. [57].

Temperature responsive capsules were also assembled using LbL approach. Prevot et al. reported such assembly where PNIPAM was encapsulated was LbL coated with PSS/PAH LbL shell. Dependence of LCST on different amount of salt added is observed and collapse of capsule is demonstrated for a drug delivery or micro sensor system [58].

In another example, PNIPAM microgel particles were coated with magnetic nanoparticles and then coated with LbL films. Multilayer assembly was achieved by PSS and PDMAC at pH 4. The system produced was found both thermosresponsive and magnetic responsive since magnetic nanoparticles are also deposited and opened the prospect of controlled drug release carrier [59,60].

Poly(2-alkyl-2-oxazoline)s (POXs) have recently attracted attention due to their both temperature responsive behaviour and important biological properties such as nontoxicity and biocompatibility [61,62]. The similarity of the chemical structure of POXs and polypeptides is the reason that they are called "pseudo-peptides". Among poly(2-alkyl-2-oxazoline)s, poly(2-isopropyl-2-oxazoline) (PIPOX) came into prominence because of the reason that its LCST is ~36^{o}C which is in range of human body making it a perfect candidate for biomedical applications [63]. Figure 1.2 shows the chemical structure of PIPOX. POXs have been also used to fabricate temperature-responsive LbL films. Erel et al. was the first demonstrating the LbL films of PIPOX and Tannic Acid (TA) via hydrogen bonding interactions among hydrogen accepting PIPOX and hydrogen donating TA [64]. Erel and co-workers also demonstrated pH- and temperature-induced release of DOX from multilayers of PIPOX and water soluble complexes of TA and DOX [65].

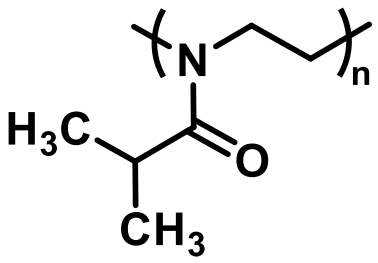

Figure 1.2 Structure of PIPOX

Multilayers of POXs other than PIPOX have also been reported. For example, the effect of temperature on the growth mechanism of LbL films of poly(n-propyl oxazoline) and TA was investigated [66]. Another study examined the

thermodynamics of LbL assembly of different types of POXs and TA [67]. Low-fouling LbL capsules has been demonstrated using POXs and poly(methacrylic acid) (PMA) [68]. Intracellular degradability and redox-responsive properties of multilayers of poly(2-ethyl-2-oxazoline) (PEOX) and PMA have also been reported [69]. Recently, LbL films of PEOX and TA containing silver nanoparticles and their anti-bacterial properties have been reported [70].

1.1.1.3 Magnetic Field Responsive Multilayers

Magnetic field responsive multilayers are widely studied across due to the ample advantage of incorporation of magnetic nanoparticles in the multilayered films for targeted drug release and imaging purposes by applying external magnetic field..

There are examples of magnetic field responsive LbL films in the literature. For example, Romero et al. fabricated Dextran containing microcapsules with LbL assembly of PAH poly(allylamine hydrochloride) and PSS poly(styrenesulphonate). The final structure of multilayer assembly was (PSS/PAH)(PSS/P(Am-DDA))-NPs (PAH)-$(PSS/PAH)_2$. These LbL capsules walls were loaded with iron oxide nanoparticles. Alternating Magnetic Field of 300 kHz, 24 kA m^{-1} was applied to the capsules for release of dextran [71].

In another study, Lu et al. fabricated LbL capsules for magnetic field triggered release of Dextran. LbL capsules were produced using poly (styrenesulphonate) (PSS) and poly (allylamine hydrochloride) (PAH) and cobalt nanoparticles were introduced in the capsule. Dextran was released at 150 kHz [72,73].

The basic phenomenon in releasing drug through magnetic field application is the oscillatory motion of the magnetic particles imbedded inside so that the polymer layers are mechanically ruptured. In general, the applied frequency varies from 50 kHz to 300 kHz to induce release of functional molecules from magnetic field responsive LbL capsules. It was reported that mostly the permeability of capsule wall was increased

around 50-150 kHz [74]. Beyond 300 kHz the permeability of polyelectrolyte capsule walls doesn't increase. Composition of magnetic nanoparticle and specific absorption ratio are the main factors affecting the strength of magnetic field that is required for release from the capsules [75].

Recently, magnetothermally responsive systems has been of interest specifically for cancer treatment [76]. The principle of magnetothermal response relies on hyperthermia treatment which is application of heat to destroy cancer cells. In case of magnetothermal responsive systems, heating the cancer tissue is provided via application of magnetic field using magnetic nanoparticles and the damage on the healthy tissue was reported to be smaller compared to direct heating of the tissue [77]. It is also possible to trigger release of drug molecules when magnetic nanoparticles are coupled with drug molecules.

Combining magnetic nanoparticles and temperature-responsive polymers is also of interest to fabricate externally triggered magnetothermally responsive drug delivery systems. In these systems, hyperthermia could be activated externally by application of magnetic field leading to magnetic heating of the magnetic nanoparticles and a temperature increase in the environment which then triggers the conformational transition in temperature-responsive polymer and the drug release from the polymer platform [78]. In these systems, different from magnetic field responsive polymer matrixes described above, the release of drug molecules is induced by magnetic heating of the nanoparticles and temperature-induced conformational changes in the polymer rather than mechanically rupturing the polymer matrix. This can be considered as an advantage because mechanical forces that are applied to the polymer may not be enough to overcome the interactions and elastic modulus of polymer [79,80]. Normally the only drawback of such these systems is that payload of drug is low as compared to other stimuli systems but considerable amount of work is being done on these days to make it more effective [81].

Apart from targeted release of drug, magnetic nanoparticles are also promising for imaging purposes. Therefore, magnetothermally responsive systems which is a

combination of magnetic nanoparticles and temperature-responsive polymers display potential for theranostic applications in which therapy and diagnosis can be performed on a single platform [77].

There are studies on magnetothermally responsive polymer drug delivery systems in the literature. An example of such a delivery system was demonstrated by Ankareddi et al. Temperature-responsive PNIPAM and poly(2-hydroxyethyl methacrylate) (HEMA) is incorporated into hydrogel network with magnetite nanoparticles. Application of magnetic field induced conformational transition in PNIPAM chains inducing the release of theophylline [82].

1.2 Magnetic Nanoparticles

The term nanoparticles refer to the material with at least one dimension in nano range. Magnetic nanoparticles are the nanoparticles which are responsive to applied magnetic field and show some response to it [83]. Because of their ultra-response to applied magnetic field, there is wide range of applications of magnetic nanoparticles in field of biology, catalysis, drug delivery, therapeutic and theranostics systems [84,85].

Mainly, magnetic nanoparticles are classified in five groups according to their response to magnetic field: 1) ferromagnetic; 2) diamagnetic; 3) paramagnetic; 4) antiferromagnetic and 5) ferromagnetic which are also called super-paramagnetic.

Materials which have net magnetic moments due to unpaired electrons are termed as ferromagnetic materials. Ferromagnetic materials show significant magnetic properties and magnetic response due to ferromagnetic domains in them. Domains are the regions in the material which contain specific number of atoms and there are unpaired electrons in it which leads to magnetic moment in each domain. Magnetization vectors of all the domains are in different direction so magnetic moment is zero when vectors are added and no magnetic moment is observed when it is demagnetized. These materials magnetize along certain crystallographic axes and the phenomenon that causes them to magnetize

along that axes is called as magneto-crystalline anisotropy. Iron, Nickel and Cobalt are examples of ferromagnetic materials. Paramagnetic materials have some net magnetic moment due to unpaired electrons in an atom but the magnetic domains are absent in them. When exposed to external magnetic field, these materials experience weak magnetic field in the direction of applied magnetic field. . Magnesium, Lithium and Gadolinium are most common examples of paramagnetic materials. Diamagnetic materials have no unpaired electrons, thus they have zero magnetic moments. They have almost negligible response to an applied magnetic field because of the change in orbital motion of electrons when magnetic field is applied. When removed away from magnetic field, the orbital motion and spin of electrons restore to normal. Gold, Copper, Silver, Zinc and Lead are examples of diamagnetic materials. Antiferromagnetic materials have two identical sub-lattices of magnetic ions. Both of these lattices are magnetized, their magnetic moments are equal in magnitude but opposite in direction. So antiferromagnetic materials have no net magnetization and the response is similar to paramagnetic materials. Manganese oxide, nickel oxide, cobalt oxide are examples of antiferromagnetic materials [83,86]. Superparamagnetic materials are all single domain particles because the size of particle is reduced. When size is reduced the coercivity first increases, however decreases after a particular radius and eventually drops to zero. This corresponds to reduction in anisotropy energy with size. Magnetic moment of each particle can be pointed at any direction and this phenomenon is called as superparamagnetism [86,87].

There are different types of magnetic nanoparticles which have been studied for biomedical applications. Examples to them are cobalt ferrite (Fe_2CoO_4) and chromium dioxide (CrO_2) [88]. Magnetic hybrid of cobalt ferrite nanoparticles and nano tubes is found in literature for both drug delivery and magnetic resonance imaging purposes [89].

Along with biological applications, magnetic nanoparticles have vast range of application in field like magnetic fluid, catalysis, data storage and magnetic resonance imaging [90]. Among all magnetic nanoparticles, iron oxide nanoparticles are ubiquitous because of their super paramagnetic behavior and the wide range of biological applications that they find use in. The main advantage of using iron oxide nanoparticles for biomedical

applications is that they show superparamagnetic behavior which reduces the chance of particle aggregation [88]. The other advantage is the size which is much smaller than the size of a cell which varies from 10-100 μm or virus which varies from 20-450 nm, making iron oxide nanoparticles perfect materials in getting close to any biological entity. Superparamagnetic iron oxide nanoparticles are perfect carriers for drug delivery applications since their motion can be controlled externally. There has still been a lot of research ongoing in use of iron oxide nanoparticles in hyperthermia treatment. Importantly, iron oxide nanoparticles are less toxic compared to the rest of magnetic nanoparticles used for biological applications, making them a preferable for biomedical applications [91,92]. There are two types of iron oxide nanoparticles: magnetite and maghemite which are (Fe_3O_4) and (γ–Fe_2O_3), respectively. These both have cubical spinal structures.

Magnetite is known as black iron oxide or Hercules stone as it is mostly found blackish in color. It consists of divalent and trivalent Fe ions. It exhibits the strongest magnetism of any transition metal oxide [93]. Magnetite has inverse spinal structure. 1/3 of the Fe is tetrahedrally coordinated with oxygen while 2/3 of the interstices are octahedrally coordinated. Tetrahedral spaces are taken by divalent ion of Fe while octahedral spaces are taken by equal amounts of divalent and trivalent ions.

Maghemite have different symmetries as compared to magnetite depending on the degree of ordering of vacancies. It is sometimes considered as fully oxidized magnetite. Oxidation is achieved with removing some Fe from structure and vacancies are being created. This is observed as a color change from blackish to red brown [94,95].

1.2.1 Synthesis of super paramagnetic iron oxide nanoparticles

Various techniques are available for synthesis of iron oxide nanoparticles in the literature, e.g. chemical Vapor Deposition method, co-precipitation method, thermal decomposition method [96]. Most convenient among all is the liquid phase co-precipitation method. It is inexpensive and it is easy to carry out with better yield [93,97].

Magnetite is usually obtained by co-precipitation of iron salts which are either iron chlorides or iron sulfates. The first magnetite synthesis via co-precipitation method was performed by Massart in 1981 [98]. The main reactions in this synthesis were as follows:

$$(Fe^{+3}(H_2O)_6)^{+3} \rightarrow \quad FeOOH + 3H^{+} + 4H_2O$$

$$Fe^{+2} + 2OH^{-} \rightarrow \quad Fe(OH)_2$$

$$2FeOOH + Fe(OH)_2 \rightarrow \quad Fe_3O_4 + 4H_2O$$

Magnetite is very sensitive to oxidation so all reactions are performed under nitrogen flow to avoid further oxidation and prevent formation of maghemite [84,86]. Nanoparticle properties such as size, shape, crystallinity and magnetic properties can be controlled by varying parameters like pH, temperature and concentration of the reagents [99].

1.3 Aim of Thesis

This thesis study aimed surface modification of iron oxide nanoparticles via LbL self-assembly technique using stimuli responsive polymers. Such LbL coated iron oxide nanoparticles can be a model study for use in theranostic applications and/or magnetothermally-induced release of drug molecules from nanoparticle surfaces.

In this respect, PIPOX was selected as the temperature-responsive component of the LbL films. As discussed in detail in Section 1.1.1.2, PIPOX, structural isomer of PNIPAM, has recently attracted great attention for biomedical applications due to its LCST-type phase behavior in the physiological range and important biological properties such as anti-fouling, and stealth behavior [63,100]. Thus, PIPOX is considered as an alternative to both PNIPAM and PEO in biomedical applications. PIPOX has carbonyl units on the pendant groups and can act as hydrogen accepting polymer in LbL assembly. pH-responsive component of LbL film was TA which is a plant polyphenol with 25 hydroxyl groups per molecule, making it an excellent hydrogen donor. LbL films of PIPOX and TA were deposited onto iron oxide nanoparticles, resulting in dual, i.e. pH- and temperature-responsive nanoparticles. Effects of polymer molecular weight, concentration of polymer solutions and deposition time on LbL coating of iron oxide particles have been investigated. DOX, a model anticancer drug was chosen to demonstrate the capability of LbL coated iron oxide nanoparticles for controlled drug delivery purposes.

Results obtained in this thesis study showed that LbL coated iron oxide particles could release DOX molecules at moderately acidic conditions and release of drug molecules is enhanced at temperatures near above body temperatures, making such nanoparticles promising platforms for magnetothermally responsive drug delivery applications. Besides, the use of iron oxide nanoparticles in imaging combined with the pH- and temperature-responsive drug release from LbL coatings make these nanoparticles promising materials for theranostic applications.

The only work reported on LbL coating of iron oxide nanoparticles concerns the use of strong polyelectrolytes, i.e. poly(styrene sulphonate) and poly(diallyldimethlyammoniumchloride) [27]. This thesis work is the first developing strategies to coat iron oxide nanoparticles with stimuli responsive polymers via LbL technique as well as to load/release drug molecules onto/from nanoparticles.

CHAPTER 2

EXPERIMENTAL

2.1 Materials

Iron(II) chloride tetrahydrate ($FeCl_2.4H_2O$), Iron(III) chloride hexahydrate ($FeCl_3.6H_2O$), ammonium hydroxide (NH_4OH) (26%), disodium hydrogen phosphate $Na_2HPO_4.2H_2O$), sodium hydroxide (NaOH) and hydrochloric acid (HCl) were purchased from Sigma-Aldrich Co. Sodium dihydrogen phosphate ($NaH_2PO_4.2H_2O$) and Tannic Acid (M_w=1701) were bought from Merck Chemicals. Doxorubicin hydrochloride was bought from European Pharmacopoeia Reference Standard. The de ionized water (DI) was purified by Milli-Q System (Millipore) at 18.2 MΩ.

2.2 Synthesis of iron oxide nanoparticles

Iron oxide nanoparticles were synthesized by ultrasound based co-precipitation method. First, deaerated DI water was prepared by purging nitrogen through DI water for 30 minutes. 0.34 g $FeCl_2.4H_2O$ (1.7 mmol) and 0.95 g $FeCl_3.6H_2O$ (, 3.5 mmol) were added to a three necked round bottom flask, followed by addition of 20 mL of deaerated DI water. The flask was subjected to ultra-sonication for 30 minutes. The mixture was continuously purged with nitrogen during this period. The mixture under constant nitrogen flow was then heated up to 50°C and then kept at 50°C for 30 minutes. Then 2 mL of ammonium hydroxide (26%) was added dropwise to the mixture. The resulting mixture was kept at 50°C for another 30 minutes and finally cooled to room temperature. Iron oxide nanoparticles were

collected by strong Nd-Fe-B permanent magnet. Particles were washed 6 times using DI water to remove the unreacted reagents and later dispersed in 20 mL DI water. The pH of iron oxide nanoparticles solution was found to be around 4 upon dispersion of the iron oxide nanoparticles in DI water [101].

2.3 Synthesis of poly(2-isopropyl-2-oxazoline)

2-isopropyl-2-oxazoline and poly(2-isopropyl-2-oxazoline) was synthesized by Eda Çağlı in our research group. Briefly, under inert atmosphere, α-bromoisobutyrl bromide was added dropwise to preheated 2-isopropyl-2-oxazoline solution in acetonitrile at 80 °C and stirred magnetically for 48 hours. Reaction was terminated with 2-butanol and purified by dialysis against water. After lyophilization, poly (2-isopropyl-2-oxazoline) was characterized by H^1-NMR and GPC.

2.4 LbL coating onto iron oxide nanoparticles

The procedure described by Wong et al.[27] was taken as a basis and then modified to coat the surface of iron oxide nanoparticles via LbL technique. The temperature was kept constant at 25^{o}C during the coating process.

5 mL of iron oxide nanoparticles solution at pH 4 was added dropwise onto 10 mL of 2.5 mg/mL TA solution (prepared in 0.01 M phosphate buffer) under ultrasonication. The ultrasonication was continued for 6.5 hours for the deposition of the first layer. 1-layer TA coated iron oxide nanoparticles were washed 3 times to remove the unbound polymer using 0.01 M phosphate pH 4 buffer by magnetic separation with a Nd-Fe-B permanent magnet. After the washing step, 1-layer coated iron oxide nanoparticles were dispersed in 10 mL of 0.01 M phosphate buffer at pH 4 and were subjected to ultrasonication for 3 hours to get a stable solution. For the deposition of the second layer, 3.0 mL of 1-layer coated iron oxide nanoparticles was added dropwise into 6 mL of 1.5 mg/mL PIPOX solution under ultrasonication. The mixture was ultrasonicated for 6.5 hours. 2-layer coated iron oxide particles were

precipitated using a a Nd-Fe-B permanent magnet and washed 3 times with 0.01M pH4 phosphate buffer. Finally, the particles were dispersed in 10.0 mL of 0.01 M phosphate buffer at pH 4 and were subjected to ultrasonication for 3 hours to get a stable solution.

Deposition of the rest of the layers were performed in the same way as described above but the concentration of 2.0 mg/mL TA and 1 mg/mL PIPOX solution was kept for 3rd, 4th and 5th layer. Scheme 2.1 describes the LbL deposition of polymers onto iron oxide nanoparticles. Zeta potential and hydrodynamic size of the particles were measured after each layer deposition.

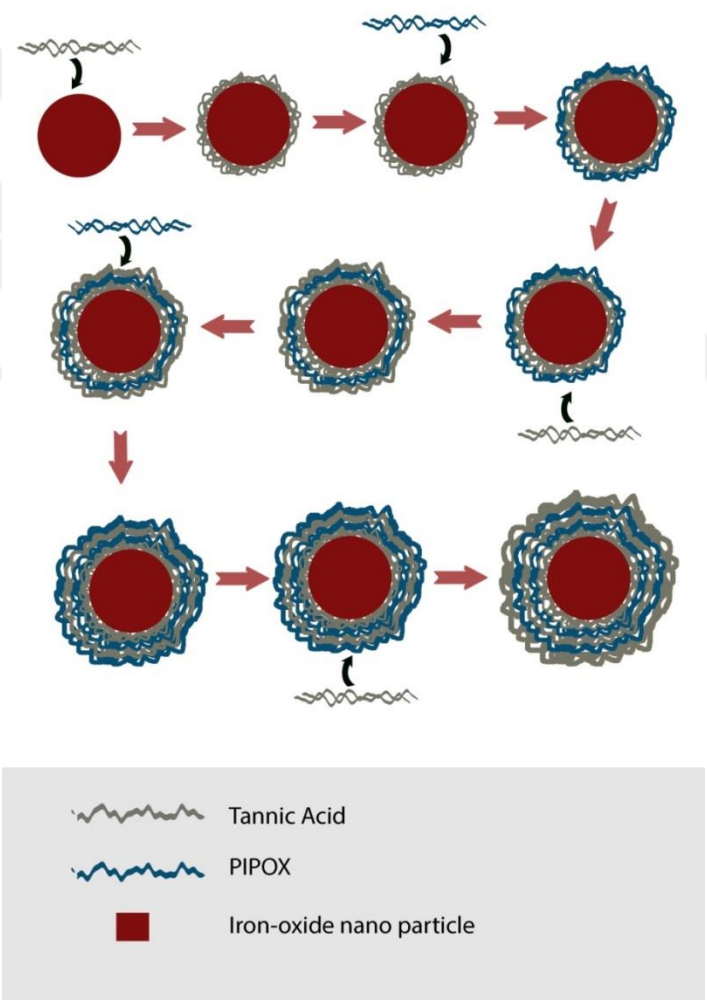

Scheme 2.1 Schematic representation of Layer-by-Layer Coating of Iron oxide nanoparticles.

2.5 DOX loading into multilayer coated iron oxide nanoparticles

pH of the 3- layer coated iron oxide nanoparticles solution was increased from pH 4 to pH 7.5. 3 mL of 3-layer coated particles at pH 7.5 was added onto 6 mL of 0.05 mg/mL DOX solution at pH 7.5 under ultrasonication and the mixture was ultrasonicated for 3 hours to load DOX molecules into 3-layer coated iron oxide nanoparticles. DOX loaded 3-layer coated iron oxide nanoparticles were washed 3 times with 0.01 M pH 7.5 phosphate buffer to get rid of the loosely bound drug molecules via magnetic separation. Finally, DOX loaded coated particles were dispersed into 3.5 mL of 0.01M phosphate buffer solution at pH 7.5 and ultrasonicated for 3 hours.

2.6 DOX release from multilayer coated iron oxide nanoparticles

Doxorubicin release was performed by dialyzing 3.5 mL of DOX loaded 3-layer coated iron oxide nanoparticles against 80 mL of 0.01 M phosphate buffer using cellulose dialysis membrane with molecular weight cut off 3500 kDa under regular mechanical stirring at 80 rpm. The pH of 0.01M phosphate buffer solution was either 6 or 7.5. The temperature of 0.01M phosphate buffer solution was kept at either 25°C or 42.5°C. At specific time intervals, 2 mL dialysate was taken out to track the release of DOX from the particles using fluorescence spectrometer.

2.7 Instrumentation

2.7.1 Dynamic light scattering and zeta-potential measurements

Hydrodynamic size and zeta potential measurements were tracked by Zetasizer Nano-ZS equipment (Malvern Instruments Ltd, UK. Hydrodynamic size was obtained by cumulative analysis and zeta potential measurements were obtained by Smoluchowski estimation.

2.7.2 pH Meter

Ohaus Starter 3000 pH meter was used for all pH adjuestments during the experiments.

2.7.3 Transmission Electron Microscopy

TEM images were obtained by FEI Tecnai G2 Spirit Bio Twin CTEM voltage 20-120 kV. Drop of iron oxide nano particles coated and uncoated was taken and air-dried on copper grid with carbon substrate.

2.7.4 X-ray Diffraction

X-ray Diffraction measurements were taken with Rigaku X-ray Diffraction (Miniflex) with CuKα (30kV, λ = 1.5405 ^{o}A). Sample was freeze dried prior to analysis and measured in the range of 20-90^{o}.

2.7.5 Fourier Transform Infrared Spectroscopy

Fourier Transform Infrared Spectroscopy was performed using a Bruner Ltd Instruments Platinum ATR attenuated total reflection. Sample was freeze dried prior to measurements.

2.7.6 Fluorescence Spectroscopy

Doxorubicin release from multilayer coated iron oxide nanoparticles was followed using a HITACHI F-2500 Fluorescence spectrophotometer. Excitation wavelength of 490 nm, scan region of 510-700nm, slith widths 5 and 10 nm were adjusted prior to measurement.

2.7.7 Vibrating Sample Magnetometry

Magnetic properties of bare and coated iron oxide nanoparticles were performed by Cryogenic Limited PPMS with Nb Ti Vibrating Sample Magnet. 300 mg of freeze dried sample were used for analysis.

CHAPTER 3

RESULTS AND DISCUSSION

3.1 Synthesis of iron oxide nanoparticles

Synthesis of iron oxide nanoparticles was performed via ultrasound based co-precipitation method using the procedure described by Szunerits et al. [102] with slight modifications. Briefly, Fe_3O_4 nanoparticles were formed by alkaline hydrolysis of the mixture of Fe (II) and Fe (III) salts according to the following reaction:

$$FeCl_2.4H_20 + 2\ FeCl_3.6H_2O + 8\ NH_4OH \rightarrow Fe_3O_4 + 8\ NH_4Cl + 20\ H_2O$$

3.1.1 Characterization of iron oxide nanoparticles

FTIR spectrum of iron oxide nanoparticles is presented in Figure 3.1. Spectrum displays a broad peak around 3370 cm^{-1} which was attributed to the vibrational stretching of hydroxyl groups at the surface iron oxide nanoparticles as well as water molecules which might have adsorbed at the surface nanoparticles. The peak at 1600 cm^{-1} was attributed to deformation modes of hydroxyl groups and water molecules. A sharp peak at 570 cm^{-1} is a characteristic of Fe-O vibration, indicating the formation of iron oxide. The peaks centered at 810 cm^{-1}1090 cm^{-1} and 1024 cm^{-1} are associated with stretching vibrations of Fe-OH [101,103].

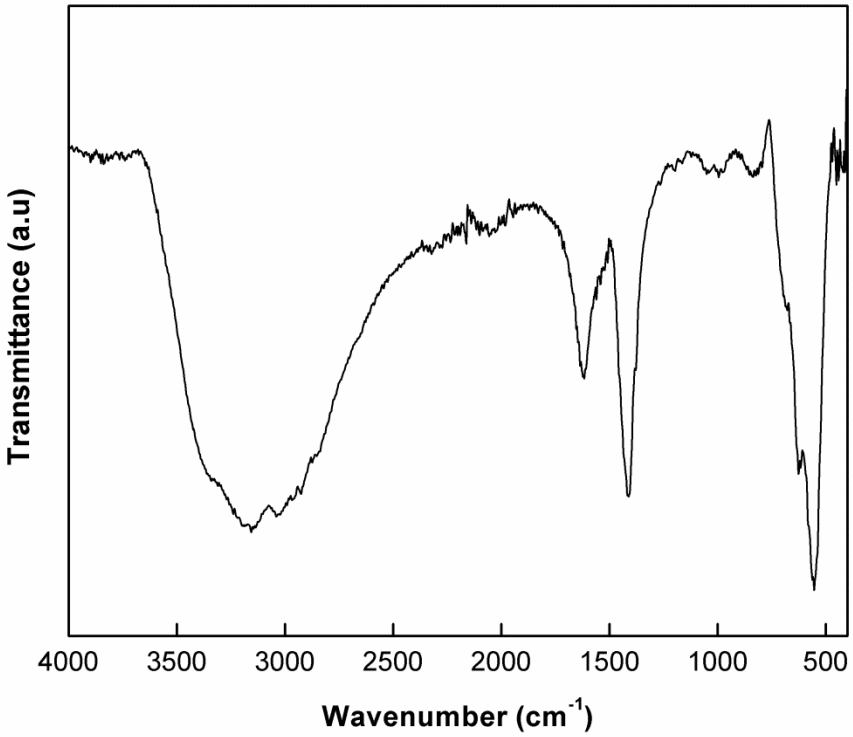

Figure 3.1 FTIR spectrum of iron oxide nanoparticles

Hydrodynamic size of iron oxide nanoparticles was measured by dynamic light scattering (DLS) technique. All the measurements were performed at 25^{o}C. The number average particle size was recorded to be 39 ± 11 nm with standard deviation of 30.1 %. The number average hydrodynamic size distribution of iron oxide nanoparticles is given in Figure 3.2. Size distribution curves obtained from several individual measurements of the same sample are represented with different colors.

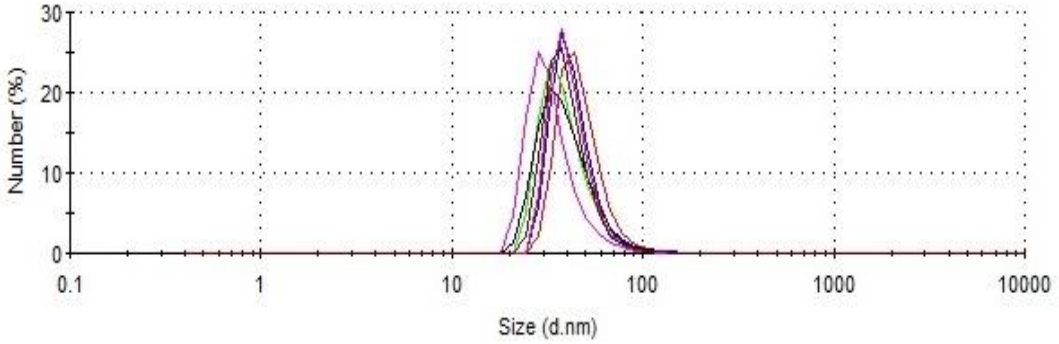

Figure 3.2 Number average size distribution of iron oxide nanoparticles. Size distribution curves obtained from several individual measurements of the same sample are represented with different colors.

Mean zeta potential of iron oxide nanoparticles was found to be ~ 42 ± 1.8 mV. Figure 3.3 shows the zeta potential distribution for iron oxide nanoparticles. The pH of the solution after synthesis was recorded as 4. Therefore, the positive zeta potential was correlated with the protonation of Fe-OH sites on the surface at acidic pH according to the following reaction:

$$Fe\text{-}OH + H^{+} \leftrightarrow Fe\text{-}OH_2^{+}$$

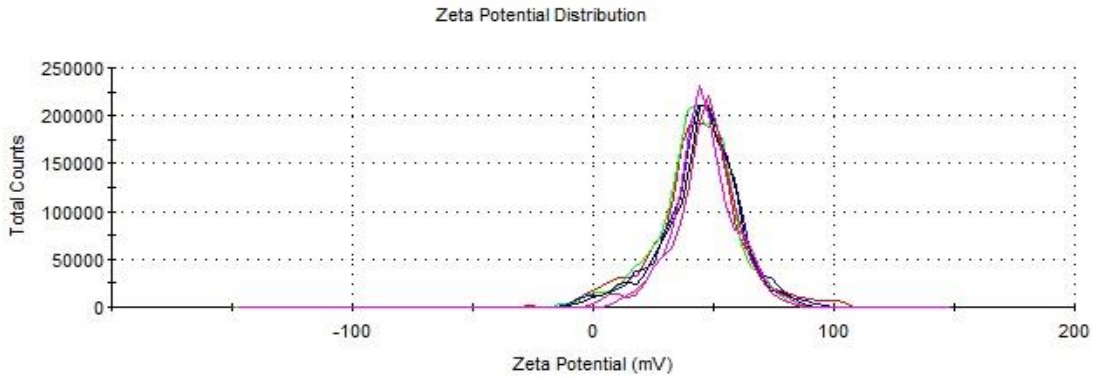

Figure 3.3 Zeta potential distribution of iron oxide nanoparticles. Zeta potential distribution curves obtained from several individual measurements of the same sample are represented with different colors.

XRD spectrum of iron oxide nanoparticles showed 4 diffraction peaks at 2θ of 30, 35.5, 57.6 and 63. These peaks correspond to [220], [311], [511] and [440] planes of

Fe_3O_4 crystals, indicating the formation of magnetite particles. The absence of the characteristic peaks of maghemite (γ-Fe_2O_3) which were [110], [210] and [211] supported the formation of magnetite particles [104]. The mean particle size by XRD analysis was determined as 8.9 nm using Scherrer Equation. The higher size values obtained via DLS was because DLS measures the hydrodynamic size, the size of the particle together with the solvent layer attached to it [105–107].

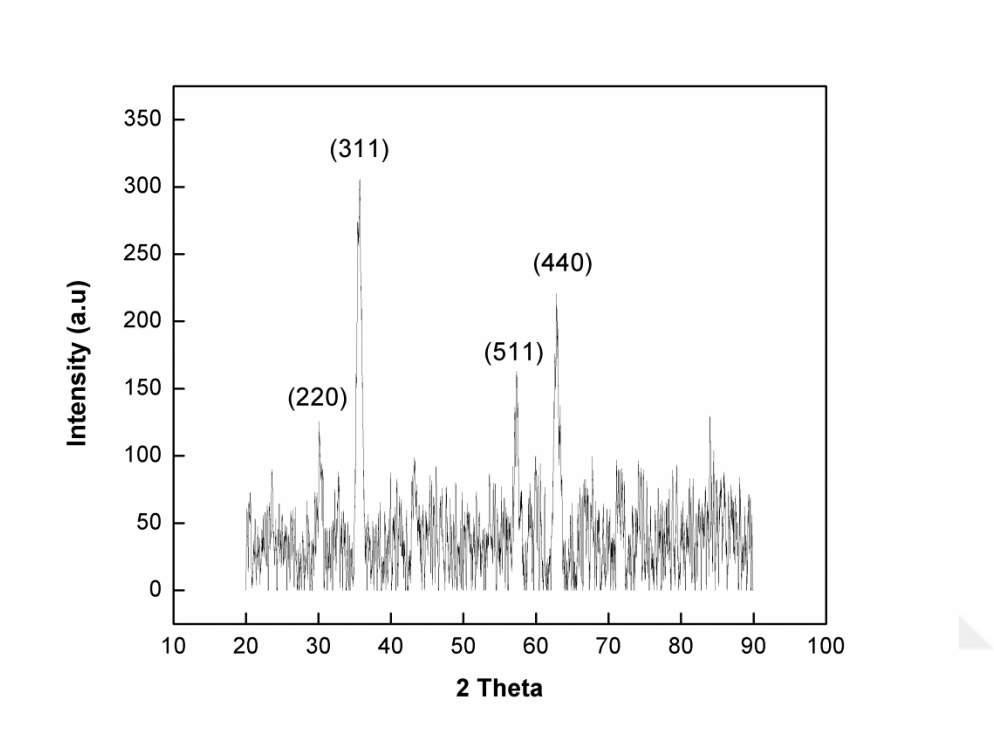

Figure 3.4 XRD pattern of iron oxide nanoparticles.

Size characterization of iron oxide nanoparticles was performed by transmission electron microscopy (TEM). Figure 3.5 shows the TEM images of iron oxide particles.

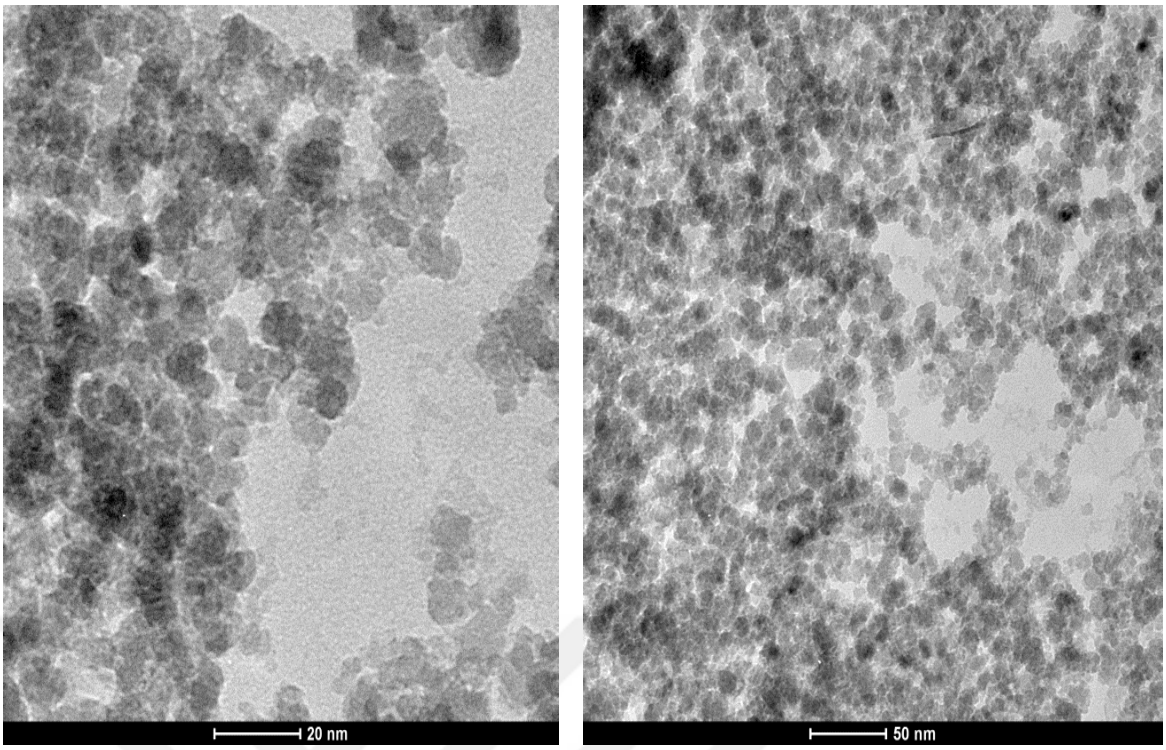

Figure 3.5 TEM images of iron oxide nanoparticles.

Most of the particles are observed with spherical shape and the diameter of the particles varied between 4 nm to 18 nm as determined by using Image J software. The average particle size of the nanoparticles was observed as 8.1 ± 1.4 nm with percent standard deviation of 27%. However, size distribution analysis via Image J software will be repeated for samples prepared using more diluted solutions of iron oxide nanoparticles.

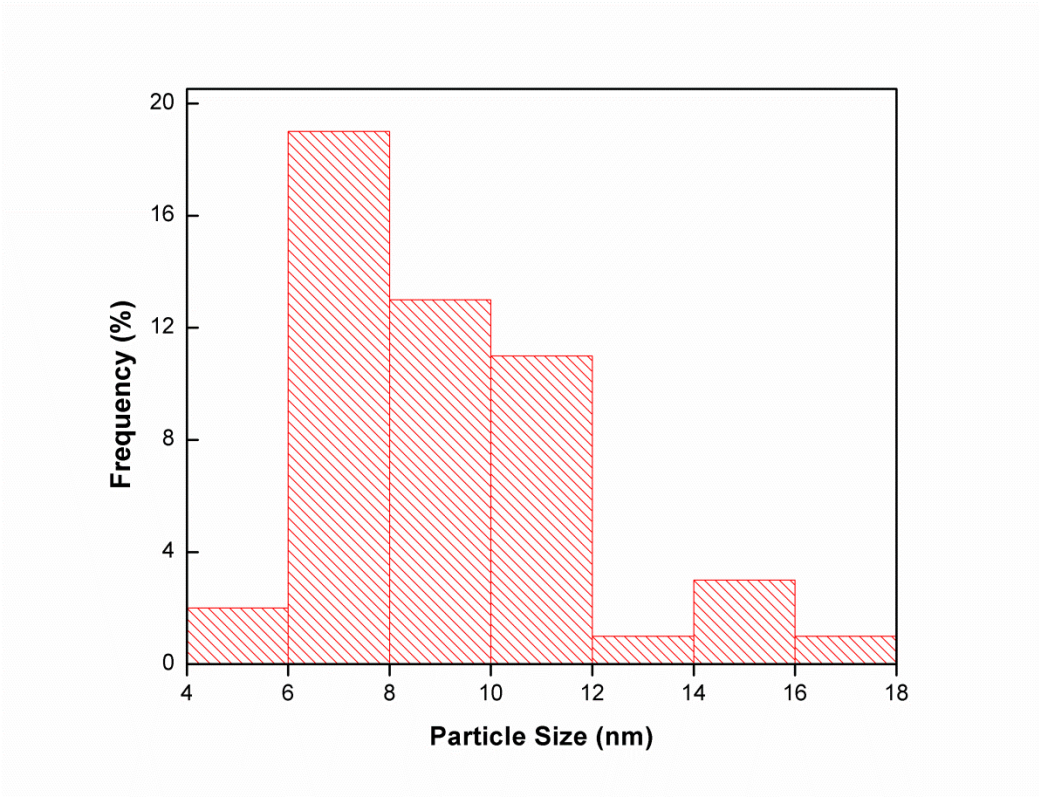

Figure 3.6 Particle size histogram of iron oxide nanoparticles from TEM images.

3.1.2 Long-term stability of iron oxide nanoparticles

At the last stage of the purification following the synthesis of iron oxide nanoparticles, the pH of the solution was recorded as 4 after dispersing the iron oxide nanoparticles in DI water. As mentioned earlier in Section 3.11, the mean number average hydrodynamic size and zeta potential of iron oxide nanoparticles was ~ 39 ± 11 nm and 42.6 ± 1.8 mV, respectively. Hydrodynamic size and zeta potential of iron oxide nanoparticles were followed every 4 hours at pH 4 and 25°C in order to track the stability of the particles in aqueous solution for a total of 72 hour period. Evolution of hydrodynamic size and zeta potential as a function of time is presented in Figure 3.7 as Panel A and Panel B, respectively.

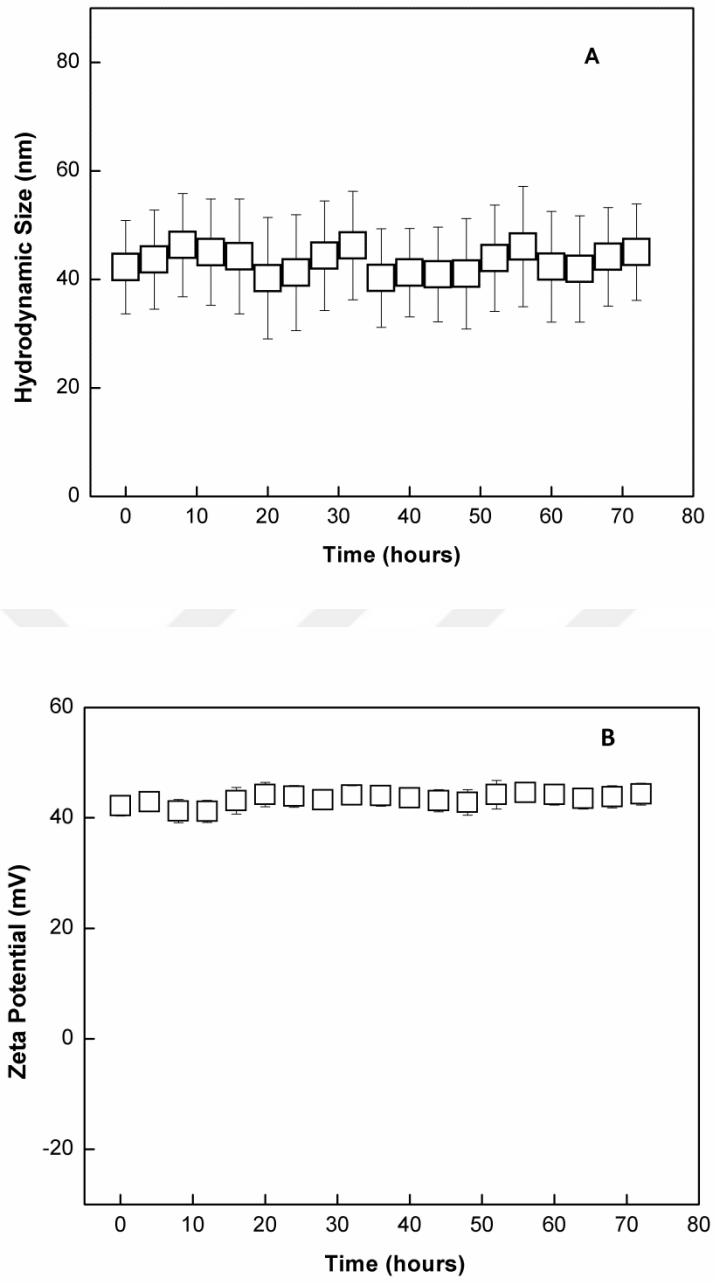

Figure 3.7 Evolution of number average hydrodynamic size (Panel A) and zeta potential (Panel B) of iron oxide nanoparticles as a function of time.

These results suggest that colloidal stability of iron oxide nanoparticles stretched up to 72 hours since no particles with significantly high hydrodynamic size which was

supposed to be the indication of aggregation were detected. The high colloidal stability of the particles was due to high zeta potential of iron oxide nanoparticles. High zeta potential is indication of strong electrostatic repulsion among iron oxide nanoparticles, preventing the aggregation.

3.1.3 pH- and temperature-stability of iron oxide nanoparticles

As mentioned in Section 1.3, aim of this thesis was to coat iron oxide nanoparticles with polymers via LbL fashion to produce nanoparticles which may have potential to be used for both imaging and drug delivery purposes. Therefore, prior to coating process, pH- and temperature-stability of iron oxide nanoparticles were followed to determine the LbL film deposition conditions.

Temperature-stability was followed between 25-50°C. Between 25-35°C and 45-50°C, the temperature was increased by 5°C steps, whereas 2.5°C increments were carried out between 35-45°C. Equilibration time was 6 minutes before each measurement. Figure 3.8 shows the evolution of hydrodynamic size as a function of temperature. No significant change in hydrodynamic size was detected between 25-50°C, providing a wide temperature range for film deposition. It is also important that iron oxide nanoparticles were stable in a physiologically related temperature range.

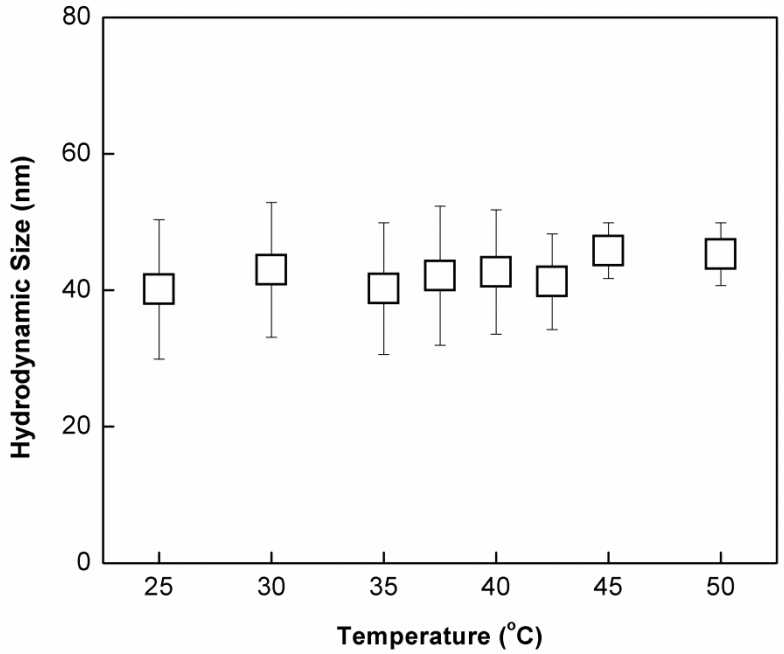

Figure 3.8 Evolution of number average hydrodynamic size of iron oxide nanoparticles as function of temperature.

pH-stability was followed by gradually increasing the pH of iron oxide nanoparticles solution and measuring both hydrodynamic size and zeta potential of the particles. As seen in Figure 3.9, the hydrodynamic size increased when the pH of the iron oxide nanoparticles solution increased from 4 to 5. A sharp increase at pH 6 was recorded due to aggregation of iron oxide nanoparticles. The hydrodynamic size further increased at pH 7, followed by precipitation of the particles. In contrast, zeta potential decreased between pH 4-6 and almost reached a value of zero at pH 7. The increasing size, in other words, aggregation of iron oxide nanoparticles as the acidity was decreased can be explained with the decrease in zeta potential and reduced electrostatic repulsion among the iron oxide nanoparticles. Deprotonation of $Fe\text{-}OH_2^+$ units at the surface of iron oxide nanoparticles with increasing pH of the solution resulted in a decrease in positive charge density at the surface, thus a decrease in zeta potential of iron oxide nanoparticles.

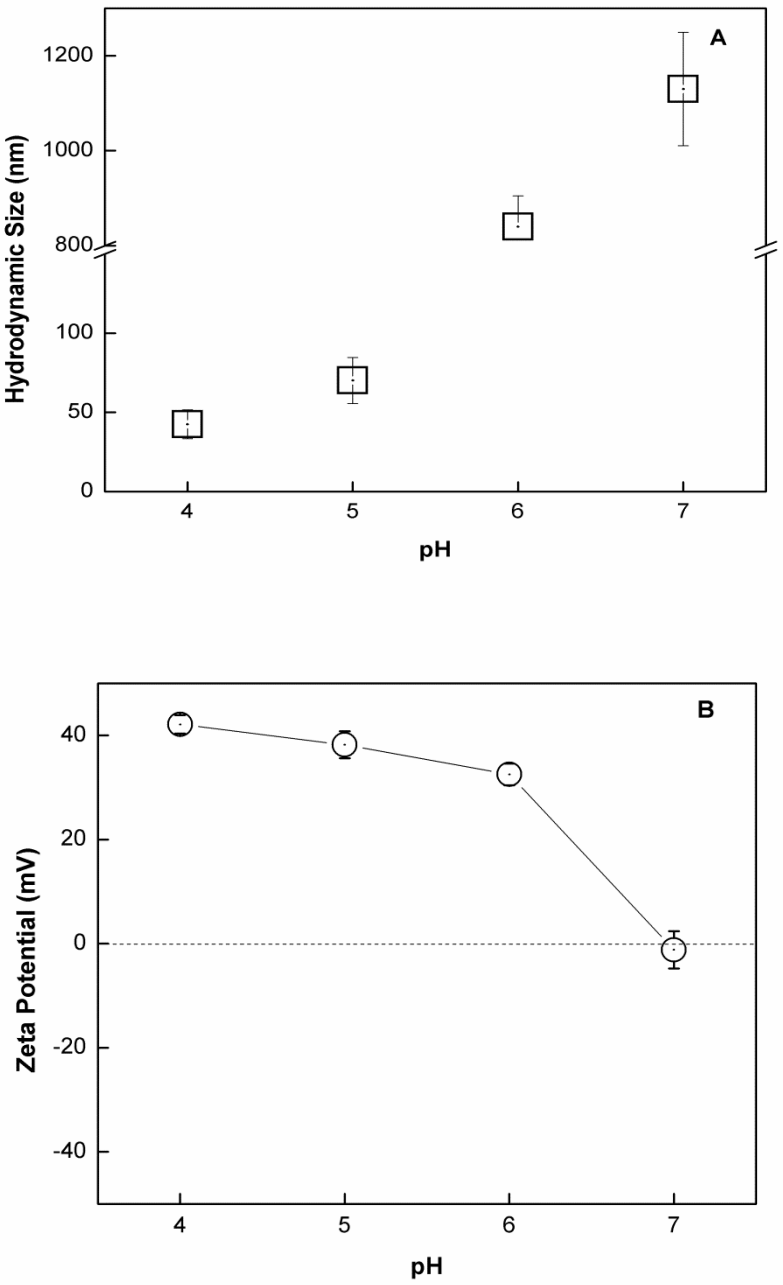

Figure 3.9 Evolution of number average size and zeta potential as a function of pH.

3.2 LbL deposition of TA and PIPOX onto iron oxide nanoparticles

Iron oxide nanoparticles were used as substrates for LbL assembly. PIPOX and TA were chosen as the hydrogen bonding polymer pairs for multilayer construction. Deposition of polymers at the surface of iron oxide nanoparticles was performed at pH 4 when iron oxide nanoparticles showed the greatest stability. Scheme 3.1 shows schematic representation of LbL deposition of TA and PIPOX onto iron oxide nanoparticles.

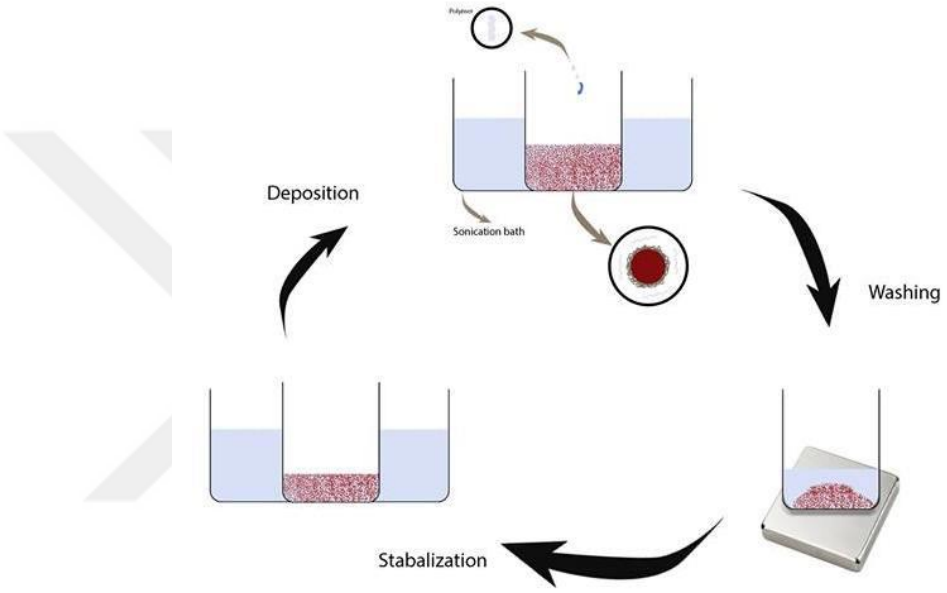

Scheme 3.1 Schematic representation of LbL deposition of TA and PIPOX onto iron oxide nanoparticles.

First layer-TA deposition

The first layer of LbL assembly was chosen as TA due to the fact that TA bears negative charge at the deposition pH (pH 4) and the interactions among positively charged iron oxide nanoparticles and negatively charged TA would be stronger than that among neutral PIPOX and iron oxide nanoparticles. TA is a polyphenol with 25

phenolic hydroxyl groups and has two pK_a values, approximated as p$K_{a,1}$= 6.5 and p$K_{a,2}$= 8.5 [65]. In the presence of positively charged iron oxide nanoparticles, ionization of TA was expected to enhance. Enhanced ionization of polyacids in the presence of salt ions or polycations has been reported before [108]. Therefore, TA has phenolate groups at pH 4 to associate with of the surface of iron oxide nanoparticles.

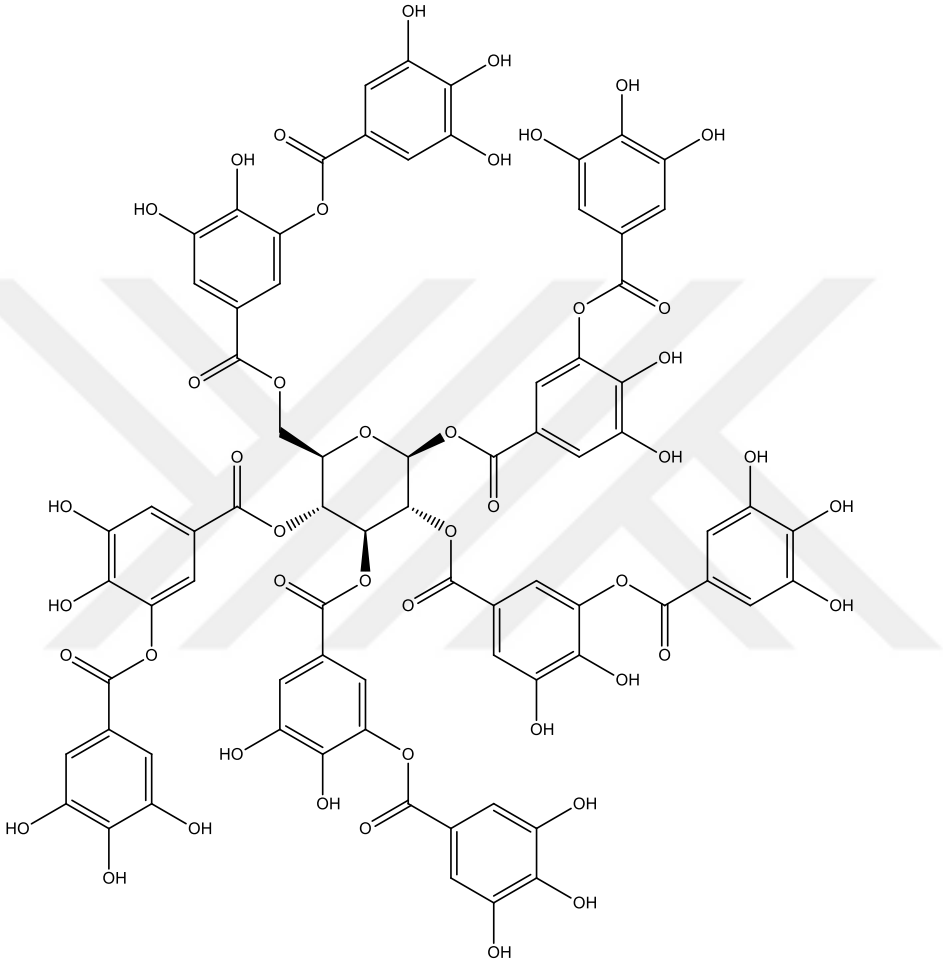

Figure 3.10 Structure of Tannic Acid.

The major difficulty with polymer deposition onto 3D substrates was to figure out the correct concentration of the polymer solution so that iron oxide particles would be coated efficiently and remain stable for a certain time after coating. Details of the effect of concentration on the stability of coated particles will be discussed later in Section 3.2.1. In summary, several TA solutions with various concentrations were

tested for coating and the concentration of TA solution was optimized at 2.5 mg/mL. Mean number average hydrodynamic size was recorded as 104.3 ± 12.2 nm and the size distribution by number of TA coated iron oxide nanoparticles is presented in Figure 3.11. Of note, the rate of TA addition onto iron oxide nanoparticles and the deposition temperature were both critical on preparation of TA modified iron oxide particles with uniform size distribution. Besides measuring hydrodynamic size, TA deposition was also followed by zeta potential measurements. The zeta potential of iron oxide nanoparticles became negative upon coating with TA. The mean zeta potential decreased from 42.6 ± 2.66 mV to -33.2 ± 1.8 after deposition of a layer of TA due to compensation of the positive charge on iron oxide nanoparticles by phenolate groups of TA. Figure 3.12 shows the zeta potential distribution for TA coated iron oxide nanoparticles. There are examples of TA coated iron oxide nanoparticles in the literature. However, these studies differ from the one described here above in the sense that TA was coated onto iron oxide particles during the synthesis step [109].

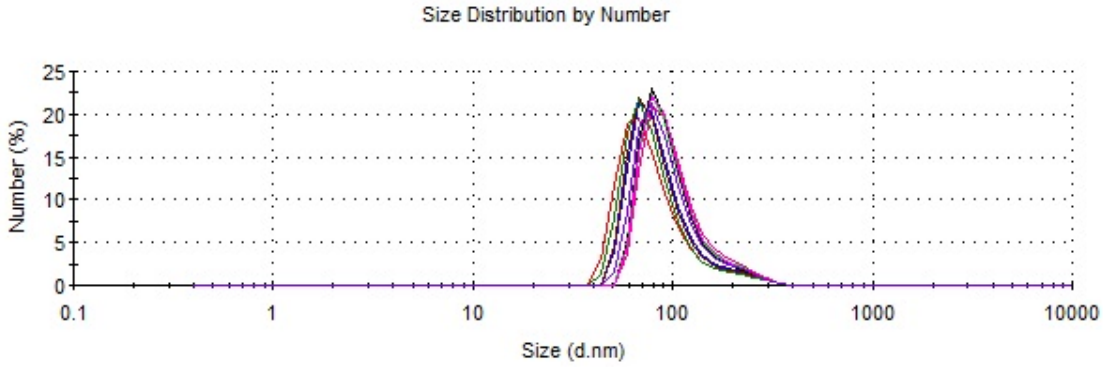

Figure 3.11 Size distribution by number of TA coated iron oxide nanoparticles. Size distribution curves obtained from several individual measurements of the same sample are represented with different colors.

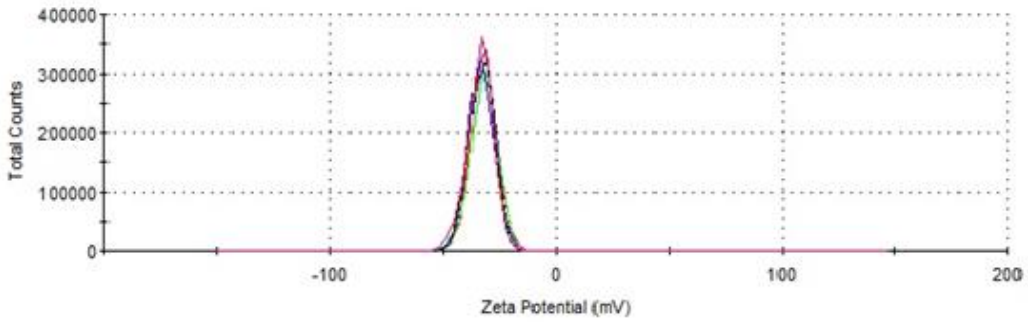

Figure 3.12 Zeta potential distribution of TA coated iron oxide nanoparticles. Zeta potential distributions obtained from several individual measurements of the same sample are represented with different colors.

Second layer-PIPOX deposition

PIPOX was deployed as the second layer onto TA coated iron oxide nanoparticles at pH 4. As explained in Section 1.1.1.2, PIPOX is a temperature responsive polyamide with hydrogen accepting nitrogen and carbonyl units. Concentration of PIPOX solution was optimized at 1.5 mg/mL using PIPOX with a Mn of 7000. The driving force for deposition of PIPOX onto TA-iron oxide nanoparticles was hydrogen bonding interactions among primarily carbonyl groups of PIPOX and phenolic hydroxyl groups of TA. Scheme 3.2 shows schematic representation of 2-layer coated iron oxide nanoparticles.

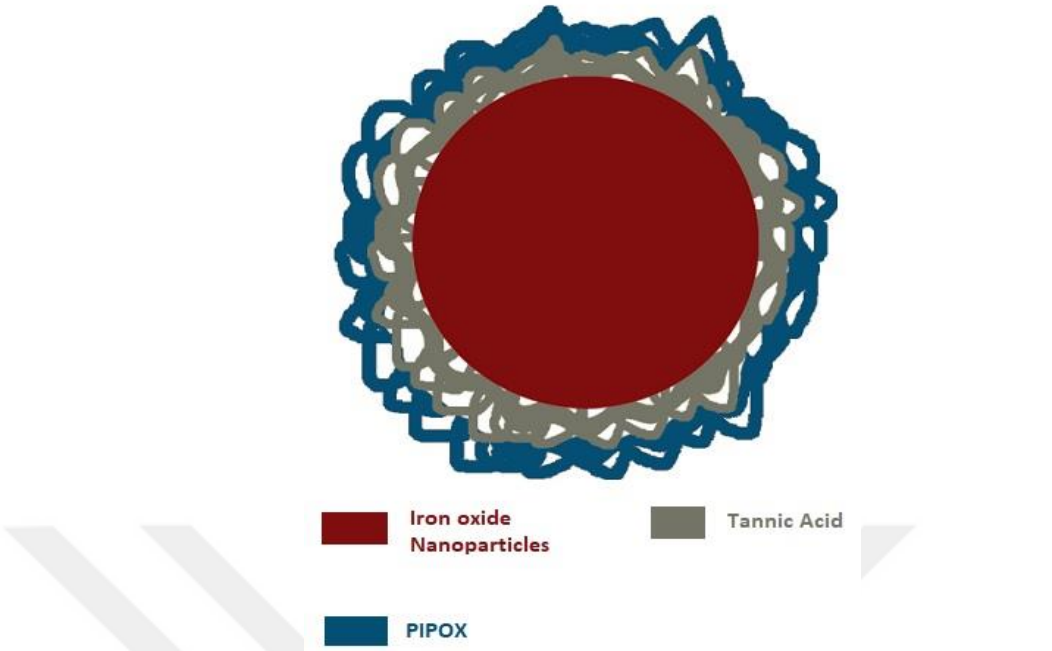

Scheme 3.2 Schematic representation of 2-layer coated iron oxide nanoparticles.

Mean hydrodynamic size of iron oxide nanoparticles-TA-PIPOX was recorded as 97.23 ± 10.21 nm upon deposition of the second layer. Figure 3.13 shows the number average size distribution of iron oxide-TA-PIPOX nanoparticles. Remember that mean hydrodynamic size of iron oxide-TA coated nanoparticles was 104.3 ± 12.2 nm. The decrease in hydrodynamic size can be due to: i) a decrease in the charge density on particles upon PIPOX deposition since the amount of ionized groups on TA was expected to be higher than PIPOX. The smaller hydration shell around the particles possibly resulted in lower hydrodynamic size; ii) PIPOX removed some of the TA that has already been adsorbed onto iron oxide nanoparticles into aqueous solution due to greater flexibility of PIPOX chains than rigid aromatic TA molecules.

Importantly, molecular weight of PIPOX and concentration of PIPOX solution were both very critical for obtaining coated iron oxide nanoparticles with uniform size. Details of the effect of concentration of PIPOX solution and molecular weight of PIPOX will be discussed later in Section 3.2.1

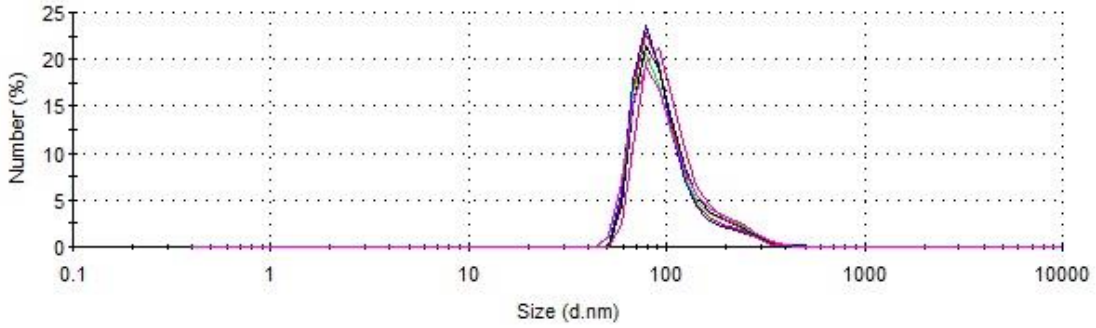

Figure 3.13 Size distribution by number for 2-layer coated iron oxide nanoparticles. Size distribution curves obtained from several individual measurements of the same sample are represented with different colors.

A noticeable drop in the mean zeta-potential was observed upon deposition of PIPOX layer. Zeta potential of the nanoparticles switched from ~ -33.2 mV to ~ -24.5 mV upon deposition of PIPOX layer. Figure 3.14 shows the zeta potential distribution for 2-layer coated iron oxide nanoparticles. In traditional LbL assembly with oppositely charged polyelectrolytes, sign of the zeta potential reverses after each layer deposition. In contrast, during the sequential deposition of TA and PIPOX onto iron oxide nanoparticles, zeta potential remained negative regardless of the nature of the polymer however became more positive upon deposition of PIPOX due to partial screening of the negative surface charge by PIPOX chains. Oscillation of the zeta potential in the negative range during preparation of capsules based on hydrogen-bonded self-assembly has been observed before [54,110].

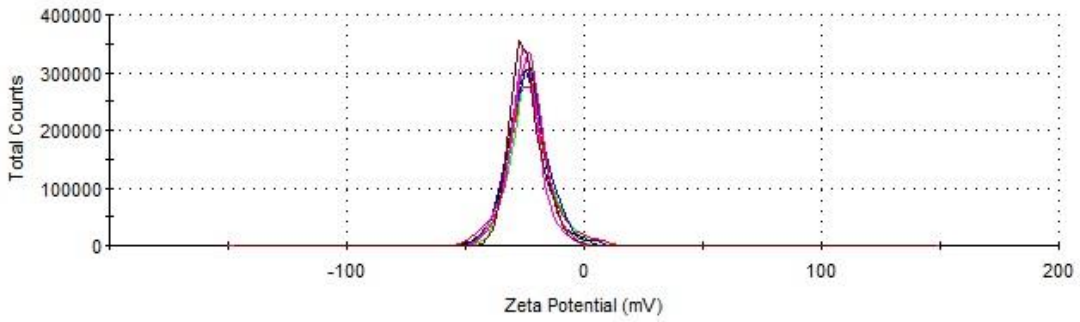

Figure 3.14 Zeta potential distribution for 2-layer coated iron oxide nanoparticles. Zeta potential distributions obtained from several individual measurements of the same sample are represented with different colors.

Third layer-TA deposition

Multilayer self-assembly onto iron oxide nanoparticles was continued by deposition of TA onto the preceding PIPOX layer at pH 4. Concentration of the TA solution was 2 mg/mL. The hydrodynamic size of the LbL coated iron oxide particles increased from 97.23 ± 10.21 nm to 105.3 ± 14.1 nm upon deposition of the third layer. This is possibly due to higher number of ionized groups on TA leading to a greater hydrodynamic size. Figure 3.15 shows the number average distribution curve for 3-layer coated iron oxide nanoparticles. Different from the distribution curves obtained after the deposition of the first and second layers, the size distribution curve for 3-layer coated iron oxide nanoparticles (Figure 3.15) was broader. This also comes out as a higher standard deviation for the mean hydrodynamic size value for 3-layer coated particles. It is important to mention that although the distribution curve became broader and particles with less uniform size were obtained, 3-layer coated particles were stable throughout the 6.5 hour of deposition time as well as stayed stable for 24 hours after deposition. The mean zeta potential switched from ~ -24.5 mV to ~ -32.9 ± 1.4 mV after the third layer deposition due to ionized phenolic hydroxyl groups of TA. Figure 3.16 shows the zeta potential distribution for 3-layer coated iron oxide nanoparticles.

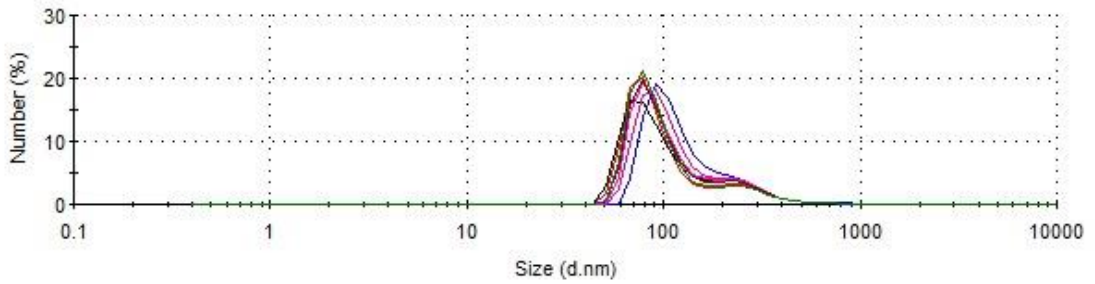

Figure 3.15 The size distribution by number for 3-layer coated particles. Size distribution curves obtained from several individual measurements of the same sample are represented with different colors.

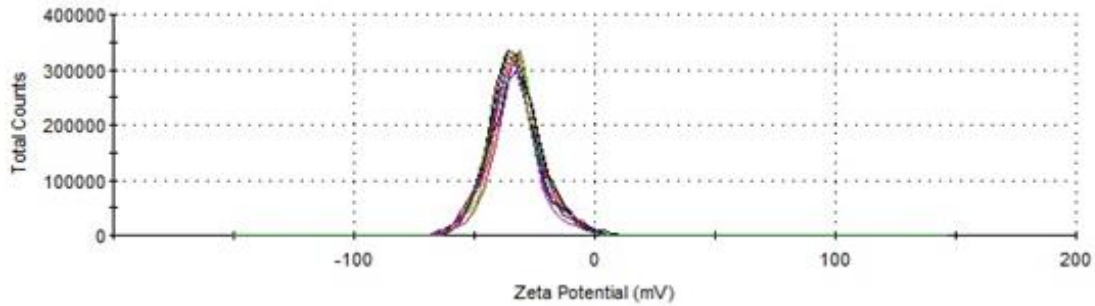

Figure 3.16 Zeta potential distribution for 3-layer coated iron oxide nanoparticles. Zeta potential distributions obtained from several individual measurements of the same sample are represented with different colors.

Fourth Layer-PIPOX deposition

PIPOX solution with a concentration of 1 mg/mL was used to self-assemble the fourth layer at the surface at pH 4. The mean hydrodynamic size was recorded as ~ 99.21 ± 13.8 nm for 4-layer coated iron oxide nanoparticles which is shown in Figure 3.17. As mentioned earlier, the small decrease in hydrodynamic size was probably due to lower number of ionized groups on PIPOX leading to a smaller hydration shell and hydrodynamic size. Similar to the zeta potential oscillation between first and second layer, zeta potential changed from ~ -32.9 mV to ~ -24.8 mV due to partial screening of the negative charge. Figure 3.18 shows the zeta potential distribution for 4-layer coated iron oxide nanoparticles. Importantly, as emphasized in the discussion of the third layer, despite the increase in the hydrodynamic size, 4-

layer coated particles showed less colloidal stability in aqueous solution both during assembly and post-assembly conditions when compared to 1- or 3- layer coated iron oxide nanoparticles where TA was the outmost layer. LbL coated iron oxide particles with PIPOX outmost layer were stable in the solution for 4 hours. This was probably due to the decrease in the negative zeta potential of LbL coated particles when PIPOX is the outmost layer.

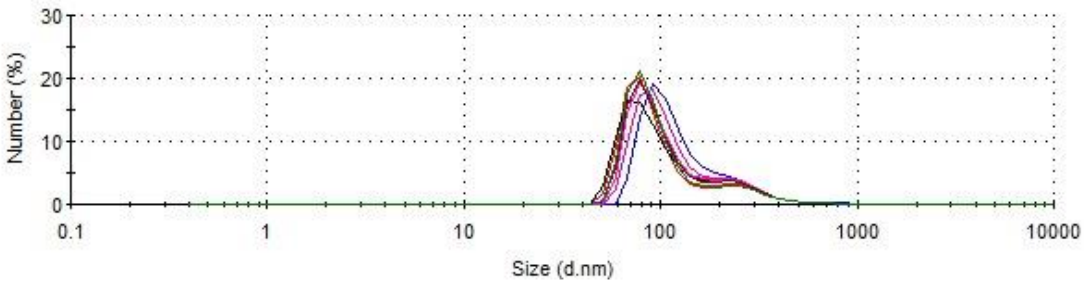

Figure 3.17 The size distribution by number for 4-layer coated particles. Size distribution curves obtained from several individual measurements of the same sample are represented with different colors.

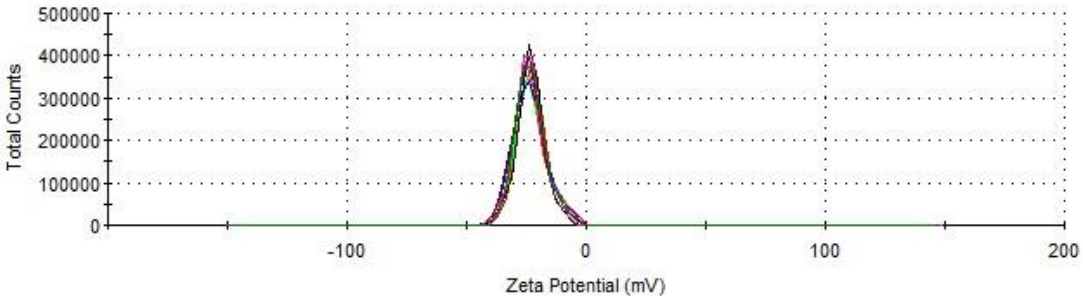

Figure 3.18 Zeta potential distribution for 4-layer coated iron oxide nanoparticles. Zeta potential distributions obtained from several individual measurements of the same sample are represented with different colors.

Fifth layer-TA deposition

Multilayer assembly was continued with TA deposition onto the preceding PIPOX layer using 2 mg/mL TA solution at pH 4. Similar to hydrodynamic size obtained after each TA deposition, hydrodynamic size increased by ~10 nm upon TA deposition. Figure 3.19 shows the size distribution by number of 5-layer coated iron oxide particles. In good agreement with the evolution of zeta-potential values observed in the previous layers, zeta potential became more negative upon deposition of the fifth layer due to phenolate groups of TA. Figure 3.20 shows the zeta potential distribution for 5-layer coated iron oxide nanoparticles.

Importantly, size distribution by number of 5-layer coated iron oxide nanoparticles was unimodal (Figure 3.19) right after the deposition; however the post-assembly stability of 5-layer coated iron oxide nanoparticles was significantly lower than 1- or 3-layer coated particles. For example, 1-layer coated iron oxide nanoparticles remained stable in aqueous solution for 48 hours, 3-layer coated iron oxide nanoparticles were stable 24 hours, whereas 5-layer coated particles remained stable in solution only for 8 hours.

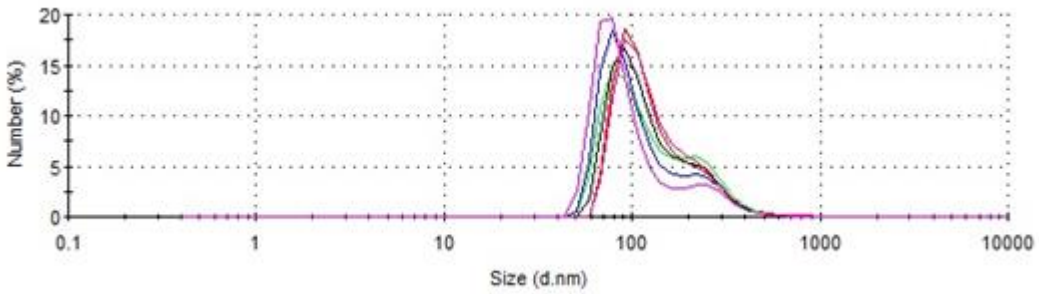

Figure 3.19 The size distribution by number for 5-layer coated particles. Size distribution curves obtained from several individual measurements of the same sample are represented with different colors.

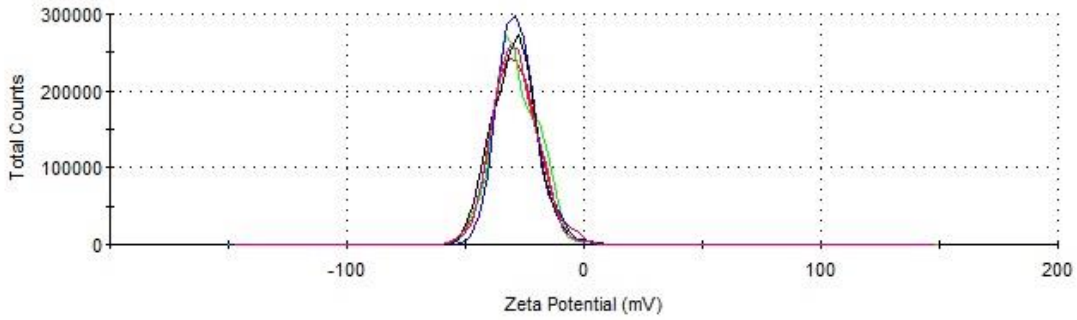

Figure 3.20 Zeta potential distribution for 4-layer coated iron oxide nanoparticles. Zeta potential distributions obtained from several individual measurements of the same sample are represented with different colors.

Sixth Layer-PIPOX deposition

Sixth layer was deposited in the same way as the second or the fourth PIPOX layers were deployed using 1 mg/mL PIPOX solution at pH 4. However, this time, size distributions obtained from several individual measurements of the same sample varied significantly from each other, indicating the presence of coated particles with significantly varying size in the solution (Figure 3.21). Zeta potential couldn't be measured as the colloidal stability was low and particles aggregated quickly after size measurements. Results obtained after the deposition of the sixth layer suggest that LbL coating process cannot be continued further and 5 was the total number of layers that could be deposited onto iron oxide nanoparticles.

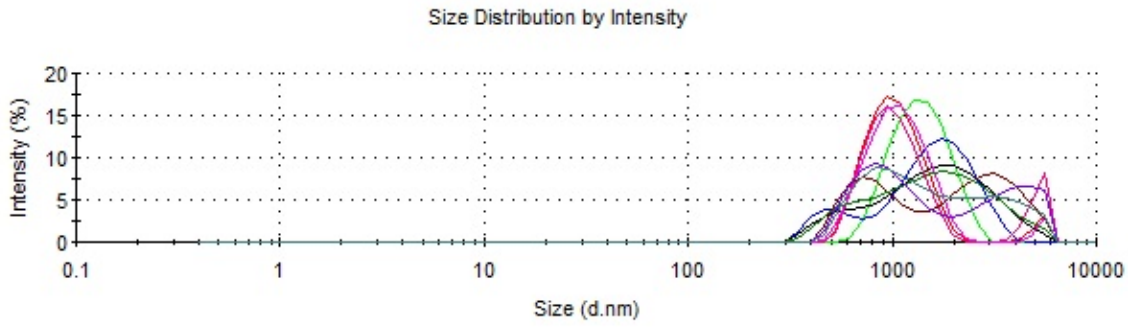

Figure 3.21 The size distribution by number for 6-layer coated particles. Size distribution curves obtained from several individual measurements of the same sample are represented with different colors.

Figure 3.22 summarizes of the evolution of the hydrodynamic size and zeta potential with increasing number of layers at the surface.

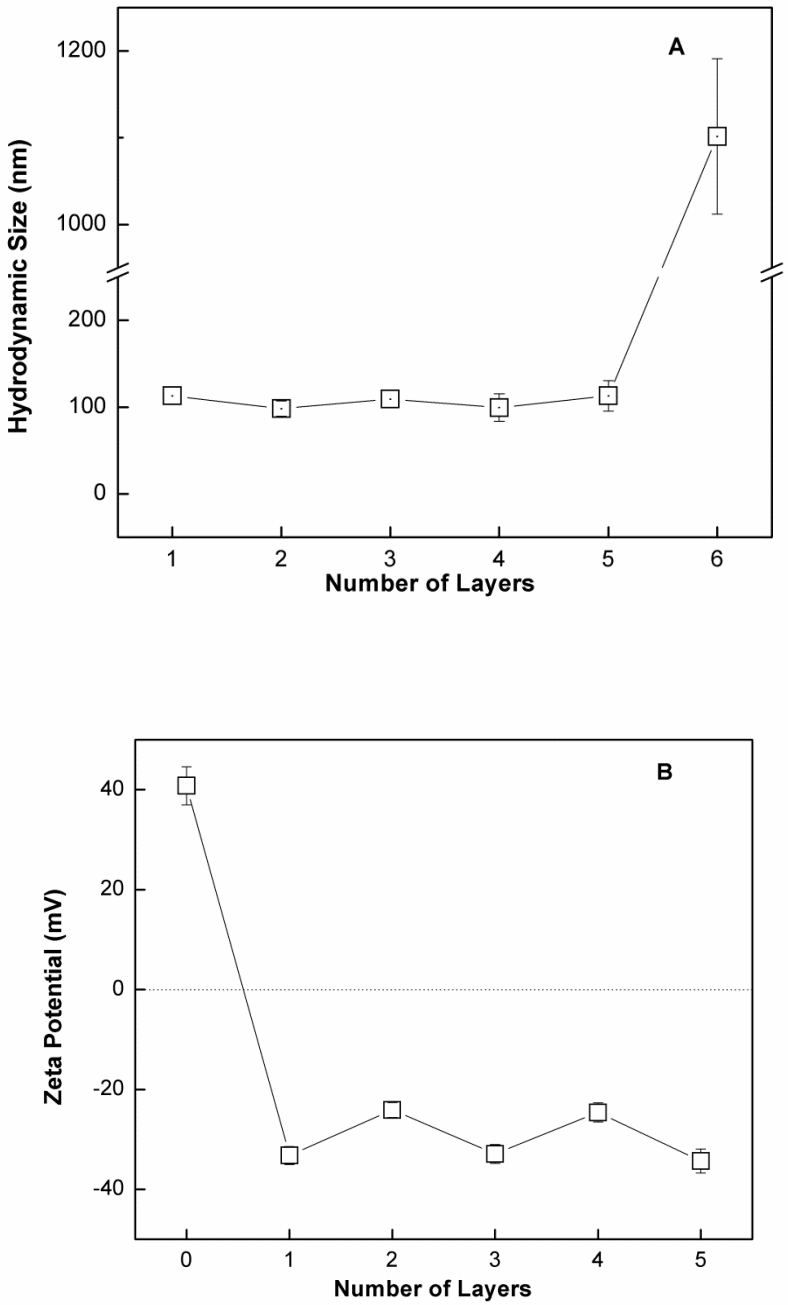

Figure 3.22 Evolution of the hydrodynamic size (A) and zeta potential (B) with increasing number of layers at the surface.

FTIR analysis of bare and LbL coated iron oxide nanoparticles

Figure 3.23 shows FTIR spectra of bare iron oxide nanoparticles, 1-layer; 2-layer and 3-layer coated iron oxide nanoparticles. The characteristic peak at 570 cm^{-1} associated with Fe-O bending vibration was observed in all spectra. In addition to the peak around 1600 cm^{-1} that is observed in the spectrum of bare iron oxide nanoparticles and associated with hydroxyl group, an additional peak merged around 1750 cm^{-1} and became sharper as the number of layers at the surface increased. The peak around 1750 cm^{-1} was correlated with ester C=O stretching vibration of TA. Similarly, multiple peaks appeared between 1000-1400 cm^{-1} which can be correlated with C-O stretching vibrations of TA as well as C-C and C-H vibrations of TA and PIPOX. The peaks became sharper with increasing layer number due to greater amount material deposited at the surface. The peaks appeared in the spectra of coated iron oxide particles were characteristic of TA rather than PIPOX. This can be explained by the greater amount of TA than PIPOX deposited at the surface [109,111].

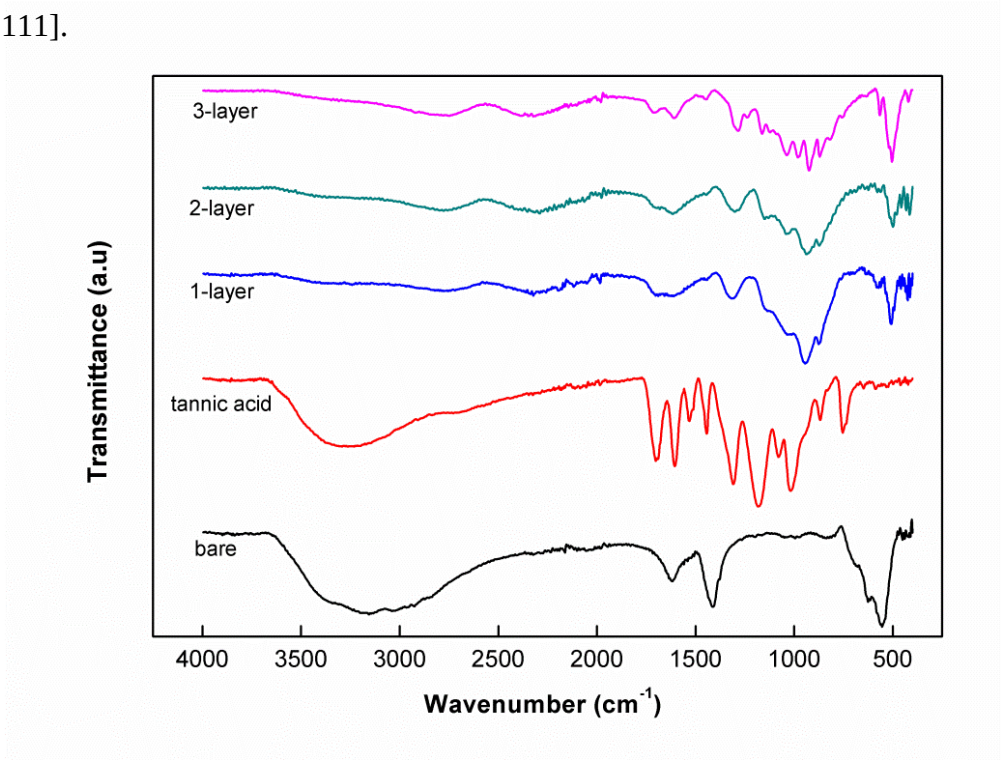

Figure 3.23 FTIR spectra of bare (black) and tannic acid (red); 1- (blue), 2- (green) and 3-layer (purple) coated iron oxide nanoparticles.

3.2.1 Effect of Molecular weight and concentration of polymer solutions on the stability of LbL coated iron oxide particles solution

It has been found that molecular weight of PIPOX was highly critical on the colloidal stability of the LbL coated particles. For example only a difference of 1400 in Mn of PIPOX resulted in aggregation of the 2-layer coated particles when the concentration of PIPOX solution was same for both cases. Figure 3.24 contrasts the number average size distribution of 2-layer coated iron oxide nanoparticles right after deposition of the PIPOX on the preceding TA layer. The dependence of the stability on the molecular weight of PIPOX may be explained by greater screening of the surface negative charge by PIPOX with higher molecular weight resulting in a decrease in the electrostatic repulsion among the particles, followed by aggregation. Alternatively, in case of PIPOX with Mn 7000, longer PIPOX chains might have associated with multiple particles, in a way acting like a bridge between the particles, eventually leading to aggregation.

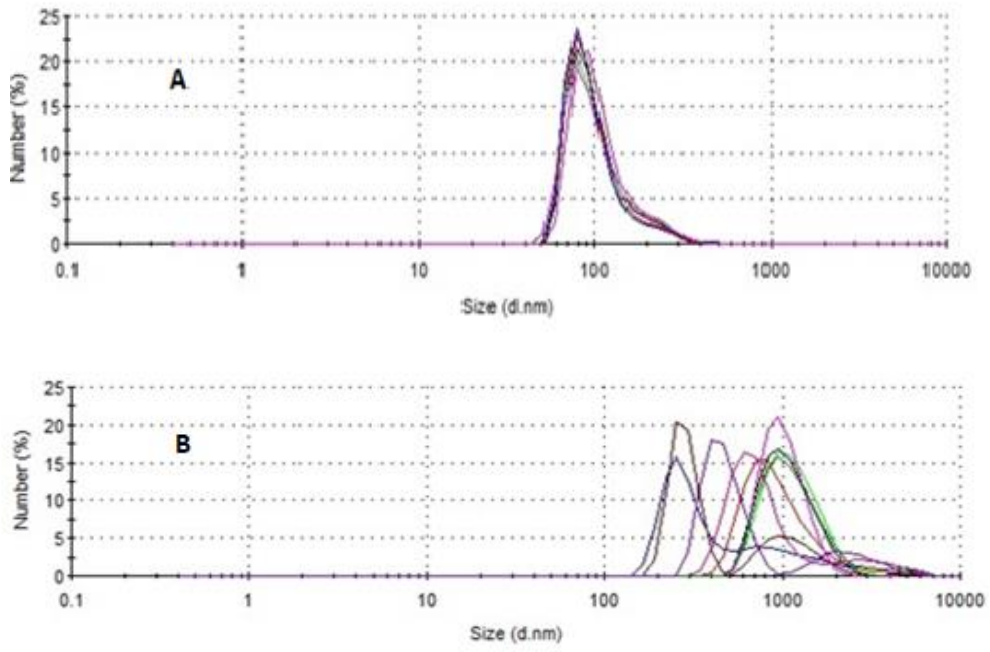

Figure 3.24 Comparison of the size distribution by number of 2-layer coated iron oxide nanoparticles when PIPOX with Mn of 5600 (Panel A) or PIPOX with Mn of 7000 was used for deposition. Concentration of the PIPOX solution was 2 mg/mL for

both cases. Size distribution curves obtained from several individual measurements of the same sample are represented with different colors.

Further trials showed that concentration of the PIPOX solution should be finely tuned when PIPOX with different Mn was used for LbL deposition. For example, it was found that the concentration of the PIPOX solution should be lowered when PIPOX with higher molecular weight was used for the stability of LbL coated iron oxide particles. Figure 3.25 contrasts the size distribution by number of 2-layer coated iron oxide nanoparticles when coating was performed with 2 mg/mL PIPOX solution using PIPOX with Mn of 5600 (Figure 3.25A) and 1.5 mg/mL PIPOX solution using PIPOX with Mn of 7000 (Figure 3.25B).

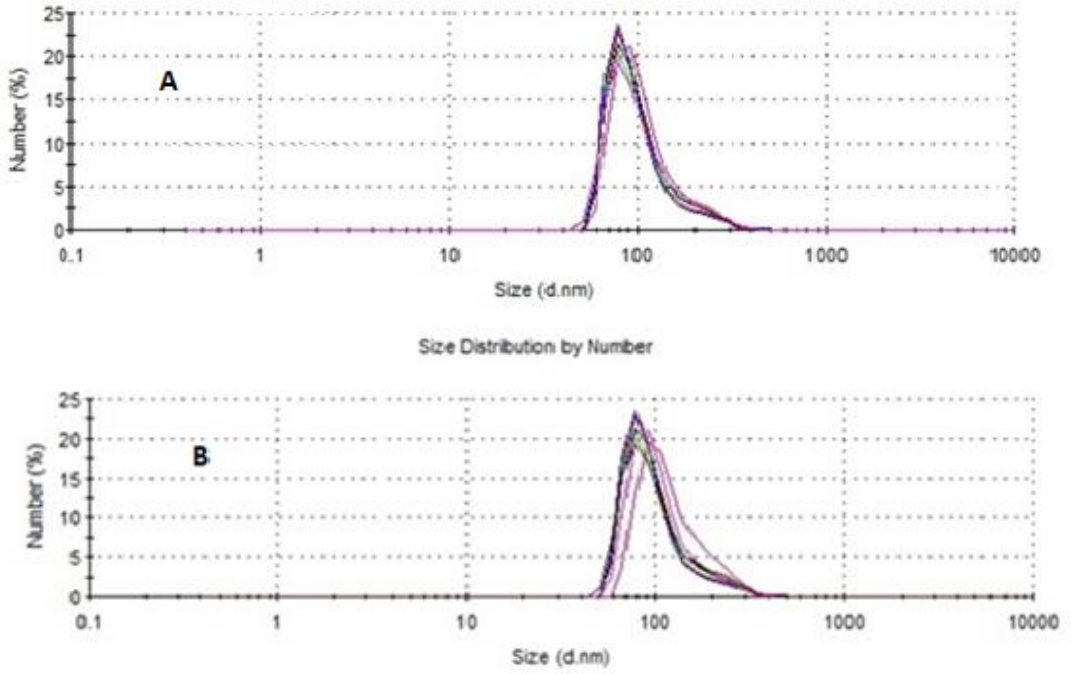

Figure 3.25 Comparison of the size distribution by number of 2-layer coated iron oxide nanoparticles when PIPOX with Mn of 5600 was used to prepare a solution at a concentration of 2 mg/mL (Panel A) or PIPOX with Mn of 7000 was used to prepare a solution at a concentration of 1.5 mg/mL (Panel B) for layer deposition. Size distribution curves obtained from several individual measurements of the same sample are represented with different colors.

Similar observations were recorded during TA deposition as well. For example, Figure 3.26 contrasts the size distribution curves of TA coated iron oxide nanoparticles using either 2.5 mg/mL (Panel A) and 3 mg/mL TA (Panel B) solutions. As seen in the Figure, a slight change in TA concentration resulted in significant difference in the size distribution of TA coated iron oxide nanoparticles. This was also obvious when standard deviations for the mean number average hydrodynamic size of two different samples were compared. The hydrodynamic size for TA coated iron oxide nanoparticles using 2.5 mg/mL and 3 mg/mL was 109.21 ± 10.2 nm and 132.1 ± 35.3 nm, respectively. 2.5 mg/mL TA solution resulted in TA coated iron oxide nanoparticles with more uniform size. Importantly, TA coated iron oxide nanoparticles which were produced using 2.5 mg/mL TA solution were stable for 24 hours, whereas TA coated iron oxide nanoparticles produced with 3 mg/mL aggregated in 12 hours.

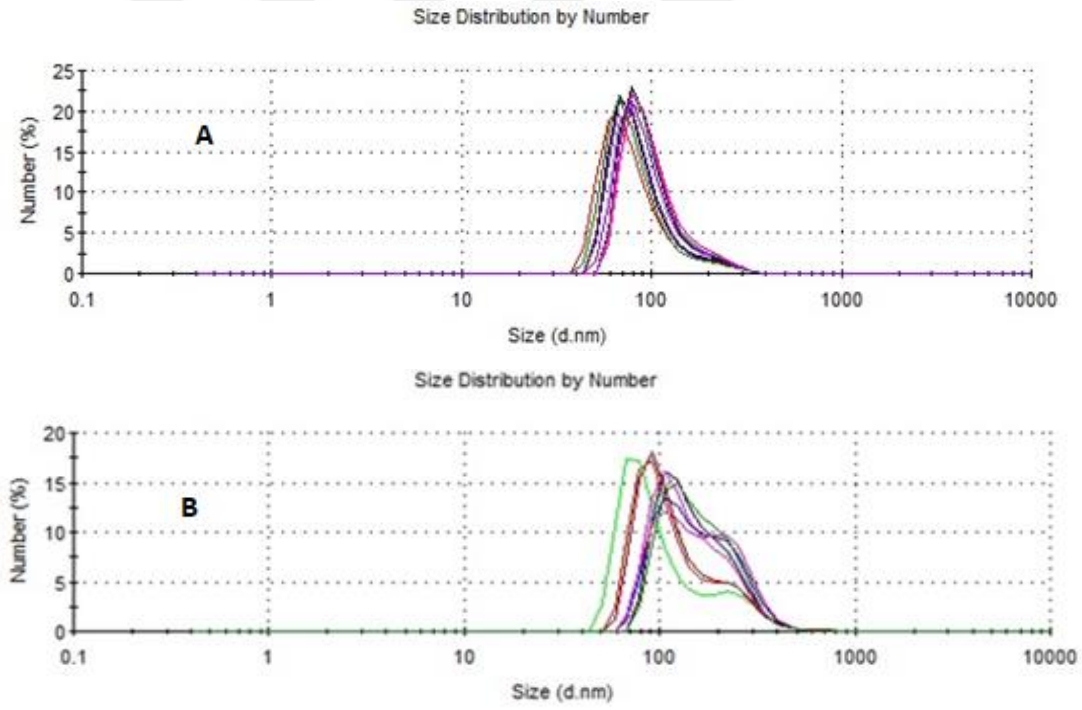

Figure 3.26 Size Distribution curve of TA coated iron oxide nanoparticles using 2.5 mg/mL (Panel A) and 3 mg/mL (Panel B) TA solution. Size distribution curves obtained from several individual measurements of the same sample are represented with different colors.

3.3 DOX loading into LbL coated iron oxide nanoparticles

DOX is an anti-cancer drug with a pK_a of ~ 8.25 [112] and it is used in this study as a model drug to examine the loading/release potential of LbL coated iron oxide nanoparticles. Chemical structure of DOX is shown in Figure 3.27

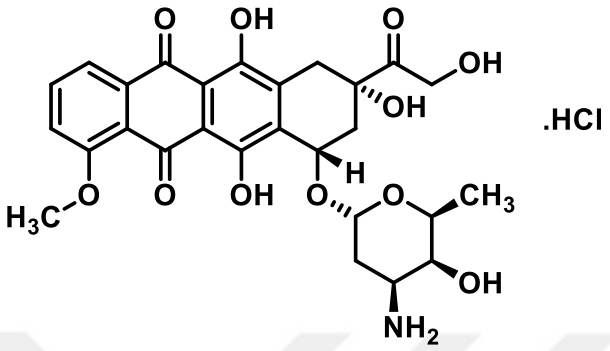

Figure 3.27 Chemical structure of Doxorubicin (DOX).

DOX loading was performed at pH 7.5. The reason to load DOX at pH 7.5 was to further ionize TA within the multilayers so that positively charged DOX could electrostatically associate with TA and absorbed/adsorbed into/onto LbL films. Besides, pH 7.5 falls into the physiological range; therefore it was hypothesized that if loading was performed at pH 7.5, DOX release at an early-stage could be minimized.

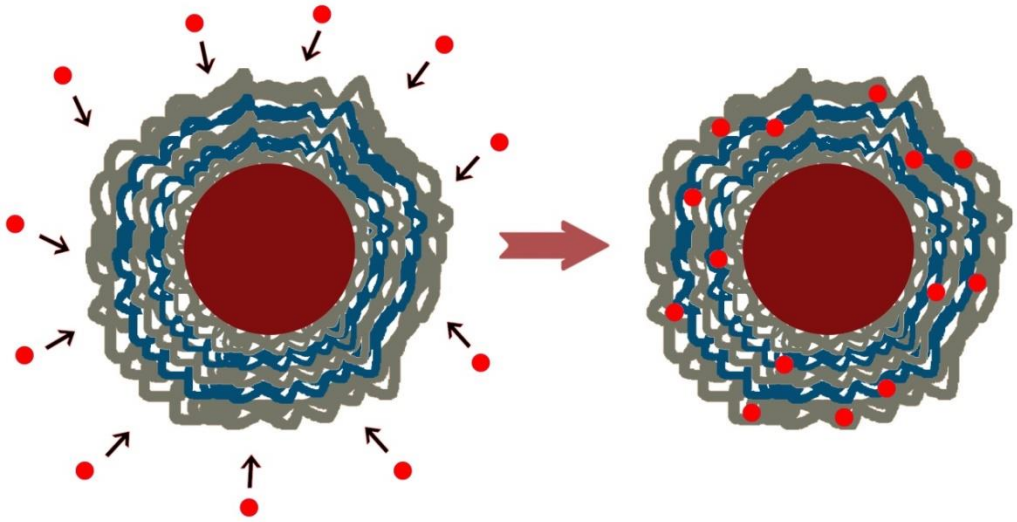

Scheme 3.3 Schematic representation of Doxorubicin loading into LbL coated iron oxide nanoparticles.

3-layer coated iron oxide nanoparticles were preferred for DOX loading/release experiments due to greater stability of these particles than that of 5-layer coated iron oxide nanoparticles. Iron oxide particles were LbL coated at pH 4 using the same procedure, discussed in Section 3.2. Then pH of the solution containing 3-layer coated iron oxide particles was increased to 7.5. The zeta potential of the LbL coated particles switched from ~ -33.2 .mV to ~ -51.4 mV, in other words, the surface charge became more negative at pH 7.5 due to further ionization of the phenolic hydroxyl groups of TA. 0.05 mg/mL DOX solution was added dropwise onto aqueous solution of iron oxide nanoparticles. The mixture was ultra-sonicated for 3 hours, precipitated using Nd-Fe-B magnet and rinsed 3 times using 0.01 M phosphate buffer solution to remove the unbound DOX molecules from the solution. The color of the supernatant turned from red to almost transparent after 3 times of rinsing. The zeta potential of the LbL coated iron oxide nanoparticles switched from ~ -51.4 mV to ~ -37.9 mV after DOX loading due to screening of the negative charge of phenolate groups of TA by positively charged DOX molecules.

Figure 3.28A shows zeta potential distribution for DOX loaded 3-layer coated iron oxide nanoparticles. Importantly, no aggregation was observed during DOX loading

process using 0.05 mg/mL DOX solution (Figure 3.28B). However, when 0.5 mg/mL DOX solution was used, particles aggregated during the loading process due to loading of greater amount of DOX molecules within the coating, resulting in a significant decrease in zeta potential of the particles, thus a decrease in the colloidal stability (Figure 3.29A and 3.29B). When 0.1 mg/mL DOX solution was used for loading, particles remained stable in the solution during the deposition process. However, duration of the colloidal stability was only 2 hours, which was shorter than that of the DOX loaded LbL coated iron oxide particles prepared using 0.05 mg/mL DOX solution.

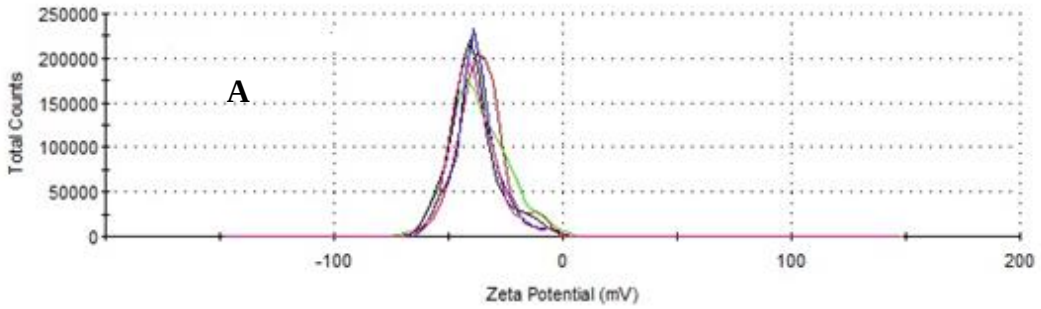

Figure 3.28A Zeta potential distribution for DOX loaded 3-layer coated iron oxide nanoparticles using 0.05 mg/mL DOX solution. Zeta potential distributions obtained from several individual measurements of the same sample are represented with different colors.

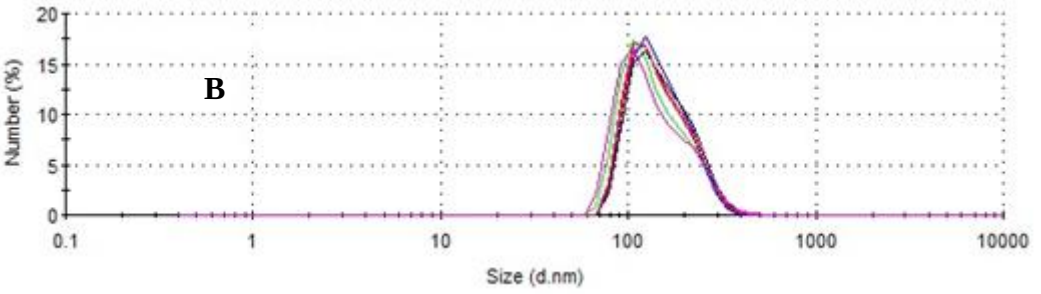

Figure 3.28B The number average size distribution curve for DOX loaded 3-layer coated iron oxide nanoparticles using 0.05 mg/mL DOX solution. Size distribution curves obtained from several individual measurements of the same sample are represented with different colors.

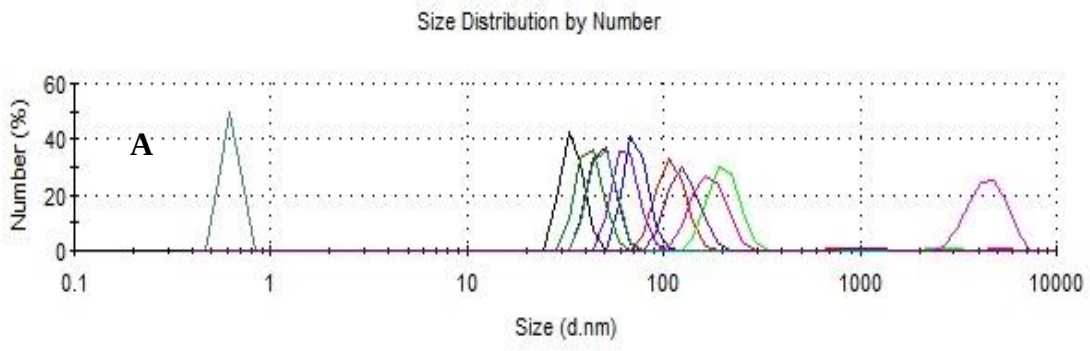

Figure 3.29A The number average size distribution curve for DOX loaded 3-layer coated iron oxide nanoparticles using 0.5 mg/mL DOX solution. Size distribution curves obtained from several individual measurements of the same sample are represented with different colors.

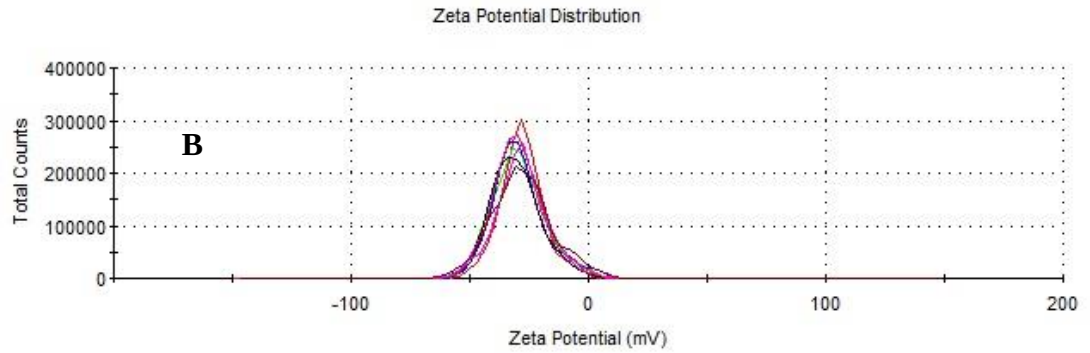

Figure 3.29B Zeta potential distribution for DOX loaded 3-layer coated iron oxide nanoparticles using 0.5 mg/mL DOX solution. Zeta potential distributions obtained from several individual measurements of the same sample are represented with different colors.

3.4 DOX release from LbL coated iron oxide nanoparticles

DOX release from 3-layer coated iron oxide nanoparticles was induced by pH- and/or temperature-trigger. DOX loaded LbL coated iron oxide nanoparticles were dialyzed against 0.01 M phosphate buffer solution under three different conditions to examine the effect of temperature and pH individually.

a) Release at pH 7.5 and 42.5°C

In this experiment, pH was kept same with the DOX loading pH to solely examine the effect of temperature on DOX release from LbL coated iron oxide particles. The temperature at which the release was performed was fixed at 42.5°C. The reason for keeping the release temperature at 42.5°C was i) to test the performance of DOX loaded LbL coated iron oxide particles as a model study for hyperthermia applications at a temperature near above body temperature and ii) to induce temperature-induced conformational changes in PIPOX above its LCST. Of note, as mentioned earlier in Section 1.1.1.2, PIPOX is a temperature-responsive polymer exhibiting LCST-type phase behavior and cloud point temperature for the PIPOX used in this study was approximated as 35°C at pH 7.5 by monitoring the intensity average hydrodynamic size of PIPOX as the temperature was increased using DLS. Figure 3.30 compares the size distribution by intensity of PIPOX at 25°C and 35°C and shows the increase in the % intensity of the aggregates at 35°C.

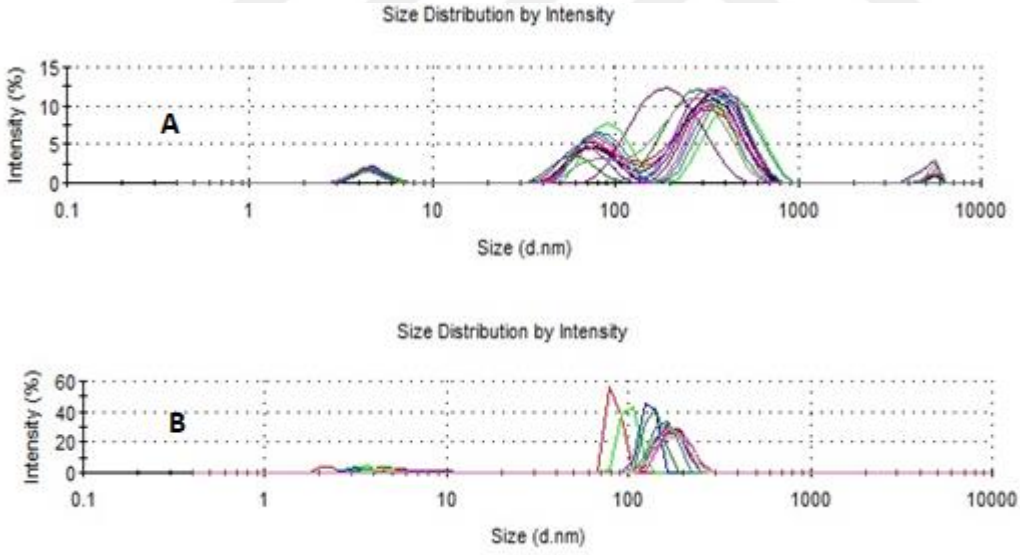

Figure 3.30 The size distribution by intensity of PIPOX at 25°C (A) and 35°C (B).

Emission spectrum of DOX has two peaks centered at 555 nm and 588 nm and DOX release from LbL coated iron oxide nanoparticles was followed by monitoring the

fluorescence intensity at 588 nm as a function of time. Figure 3.31 shows the DOX release at pH 7.5 and 42.5°C.

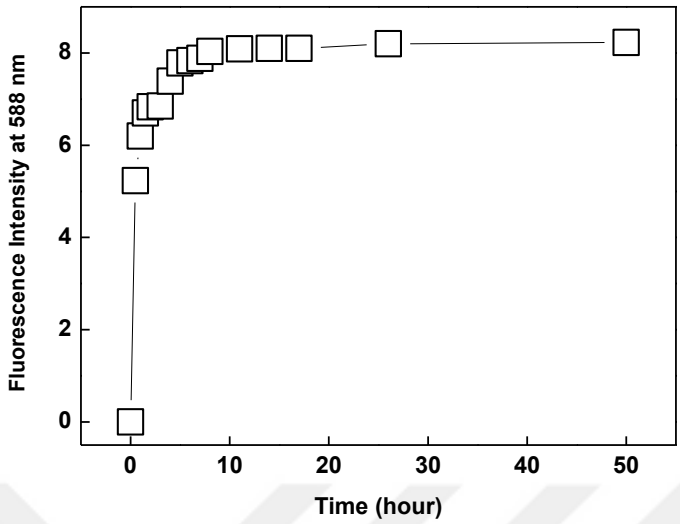

Figure 3.31 DOX release at pH 7.5 and 42.5°C from 3-layer coated iron oxide nanoparticles.

From Figure 3.31, the maximum amount of DOX that could be released is released in the first 4 hours. Release continued up to 8 hours with smaller increments compared to the first 4 hours. After 8 hours, DOX release was almost completed. Release was further followed up to 50 hours. However, no significant increase in the amount of DOX was recorded. For example, the increase in the intensity of the DOX was only 1 % and 0.5% after 26 and 50 hours, respectively when compared to the amount released after 8 hours. Under these conditions, since pH was same with DOX loading pH, DOX release can be correlated with conformational transition of PIPOX chains from extended to globular as the temperature was increased, leading to formation of void-like structures within the multilayers and facilitating the release of DOX from the multilayers. Additionally, increased kinetic energy of DOX molecules could have also resulted removal of some of DOX molecules from the multilayers. Scheme 3.4 shows the schematic representation of temperature-induced release of DOX from the surface of LbL coated iron oxide nanoparticles.

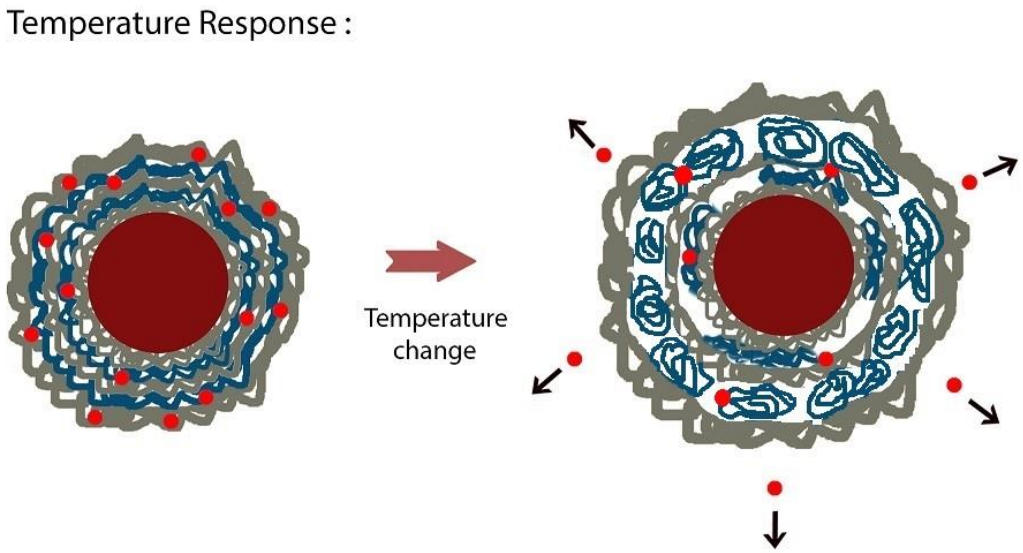

Scheme 3.4 Schematic representation of temperature-induced release of DOX from the surface of LbL coated iron oxide nanoparticles.

b) Release at pH 6 and 25°C

At these release conditions, temperature was kept same with the loading temperature which was significantly lower than the critical temperature of PIPOX. Therefore, no conformational transitions of PIPOX chains were expected. This time, pH of the release solution was kept at pH 6 which was lower than the pH of the solution at the loading step. The reason for examination of the release at moderately acidic conditions was the acidic nature of tumor tissues. Figure 3.32 shows that DOX could also be released from the surface of LbL coated iron oxide nanoparticles via only pH trigger. Importantly, DOX released much slowly from the multilayers than that under pH 7.5/42.5°C conditions. Intensity of DOX gradually increased up to 8th hour. Although, it slowed down, still significant amount of DOX was released between 8-17th hours. The release was not complete, however significantly slowed down after 17th hour. For example, the increase in the intensity of the DOX was only 2 % and 1 % after 26 and 50 hours, respectively when compared to the amount released after 17

hours. The driving force for the release of DOX from the multilayers can be explained by protonation of phenolate groups of TA as the acidity was increased and loss of electrostatic interactions among TA and DOX molecules. Scheme 3.5 shows the schematic representation of pH-induced release of DOX from the surface of LbL coated iron oxide nanoparticles.

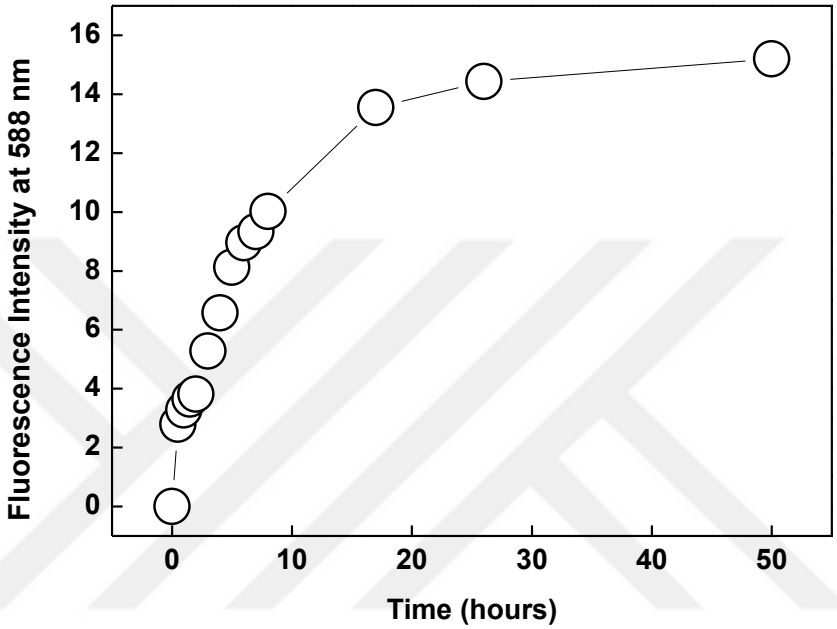

Figure 3.32 DOX release at pH 6 and 25°C from 3-layer coated iron oxide nanoparticles.

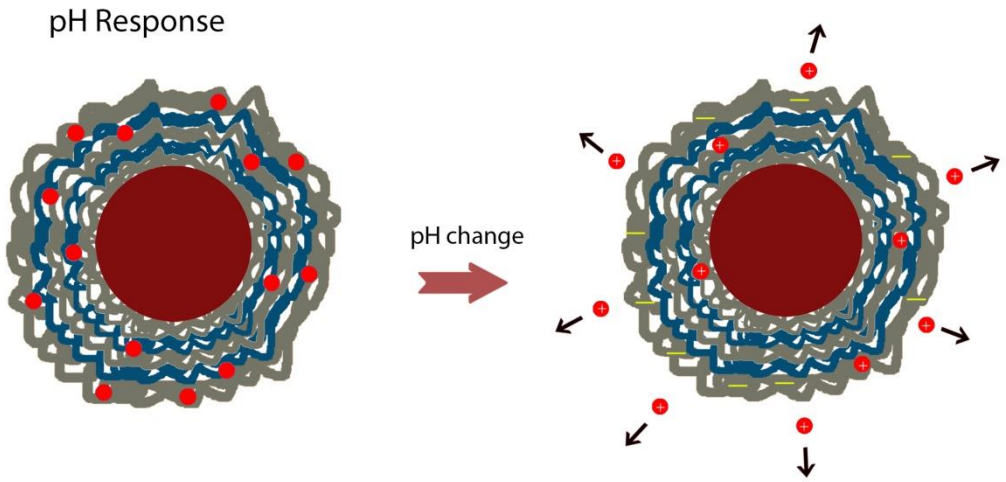

Scheme 3.5 Schematic representation of pH-induced release of DOX from the surface of LbL coated iron oxide nanoparticles.

c) Release at pH 6 and 42.5°C

Figure 3.33 shows the release under pH 6/42.5°C conditions. Here, release occurred through both pH and temperature trigger. Therefore, the driving force for release was both conformational transition of PIPOX chains leading to formation of void like structures within the multilayers so that DOX could release more easily from the surface and the loss of electrostatic interactions among TA and DOX molecules as the pH was lowered and phenolate groups of TA got protonated. As seen in the figure, majority of DOX that can be released in the first 4 hours. Released continued up to 8th hours with smaller increments. The increment got smaller between 8-17 th hours, however still continued. No significant increase in DOX intensity was recorded beyond 17 hours. The release profile observed under pH 6/42.5°C conditions was a kind of combinations of the release characteristics under pH 7.5/42.5°C and pH 6/25°C conditions.

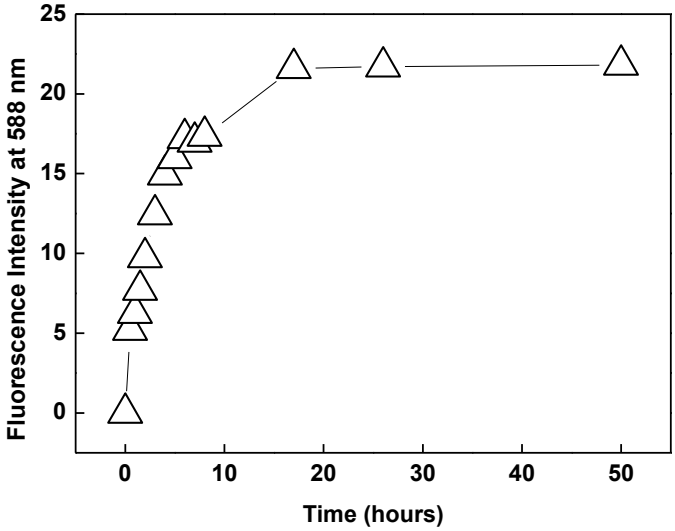

Figure 3.33 DOX release at pH 6 and 42.5°C from 3-layer coated iron oxide nanoparticles

Comparison of the release under different conditions

Fluorescence intensity of DOX is affected by the solution pH as well as the solution temperature. Therefore, for a reliable comparison of the amount of DOX released from the LbL coated iron oxide particles under different conditions, calibration curves were prepared for each condition and these curves were used to quantify the DOX released from the surface of the particles. Figure 3.34 shows the DOX released under each condition after 50 hours. Calibration curves at each condition are represented in Appendix.

The greatest release was observed at pH 6 and 42.5°C where release was triggered via both pH and temperature. A comparison of the amount of DOX released from the particles at pH 7.5/42.5°C and pH 6/25°C suggested that pH-trigger was more effective in releasing DOX from the surface of the particles. However, DOX release from the surface at 42.5°C was significantly higher than that at 25°C, indicating the effect of temperature on the amount of DOX release. Importantly, the release was

faster when DOX release was triggered via temperature-trigger rather than pH-trigger alone.

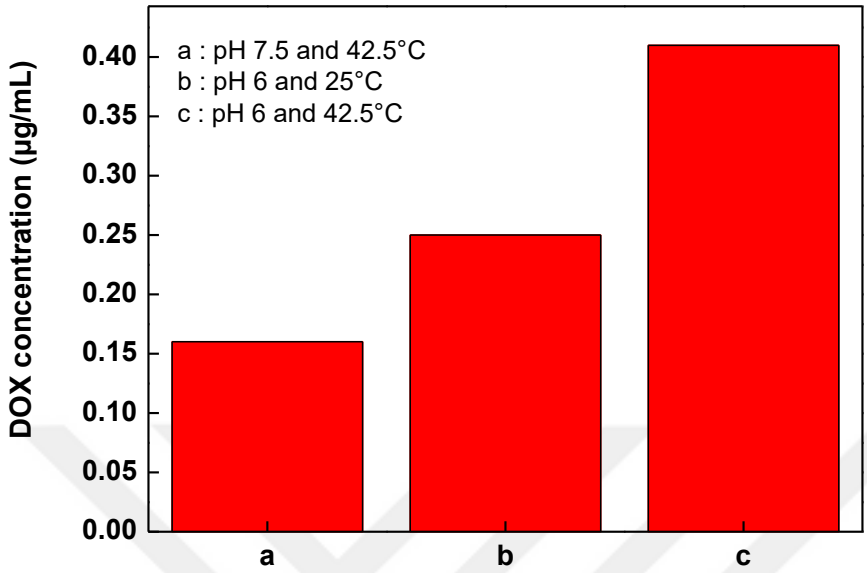

Figure 3.34 Amount of DOX released from the surface of 3-layer coated iron oxide nanoparticles at pH 7.5/42.5°C, pH 6/25°C and pH 6/42.5°C.

3.5 Magnetic Properties of bare iron oxide nanoparticles and TA coated iron oxide nanoparticles

Magnetothermally responsive nanomaterials are promising carriers for hyperthermia-triggered drug release. Magnetothermally responsive nanomaterials are generally composed by combining superparamagnetic nanostructures with thermally responsive polymers. Drug release from magnetothermally responsive nanomaterials is induced by application of AC magnetic field leading to heating of the magnetic nanoparticles and a temperature increase within the polymer matrix. The increase in temperature leads to phase separation of the temperature-responsive polymer and triggers the drug release from the polymer matrix.

In this part of the study, magnetic properties of the particles were examined to understand whether DOX loaded LbL coated iron oxide particles may have potential to be used as magnetothermally responsive drug carriers. Vibrating sample magnetometer (VSM) was used for measuring the magnetization of the particles. Figure 3.35 shows the mass magnetization (emu/g) as a function of magnetic flux density (Tesla). No hysteresis was observed, supporting the super paramagnetic behavior of iron oxide nanoparticles. The saturation magnetization of iron oxide nanoparticles reached 32 emu/g. No coercivity and remanence was observed for iron oxide nanoparticles. Magnetic nanoparticles having such properties are considered as superparamagnetic in the literature [113,114].

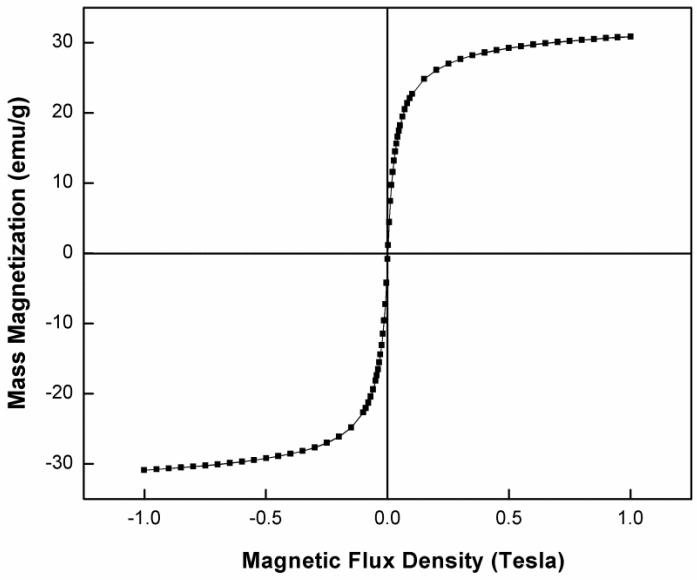

Figure 3.35 Mass magnetization vs magnetic flux density for bare iron oxide nanoparticles.

For LbL coated iron oxide nanoparticles, the question was whether iron oxide nanoparticles lose their superparamagnetic properties upon coating with polymers or not. As discussed in Section 3.2.1 in detail, the greatest hydrodynamic size increase was recorded upon deposition of the first TA-layer onto iron oxide nanoparticles. Therefore, magnetization of 1-layer coated iron oxide nanoparticles was measured and compared with the data obtained for bare iron oxide nanoparticles. As seen

Figure 3.36, no hysteresis was recorded for TA-coated iron oxide nanoparticles. Although magnetization saturation decreased from 32 emu/g to 20.2 emu/g upon coating of the first layer, TA coated iron oxide nanoparticles also exhibited superparamagnetic properties. No coercivity and remanence were observed after 1-layer TA deposition onto iron oxide nanoparticles [109].

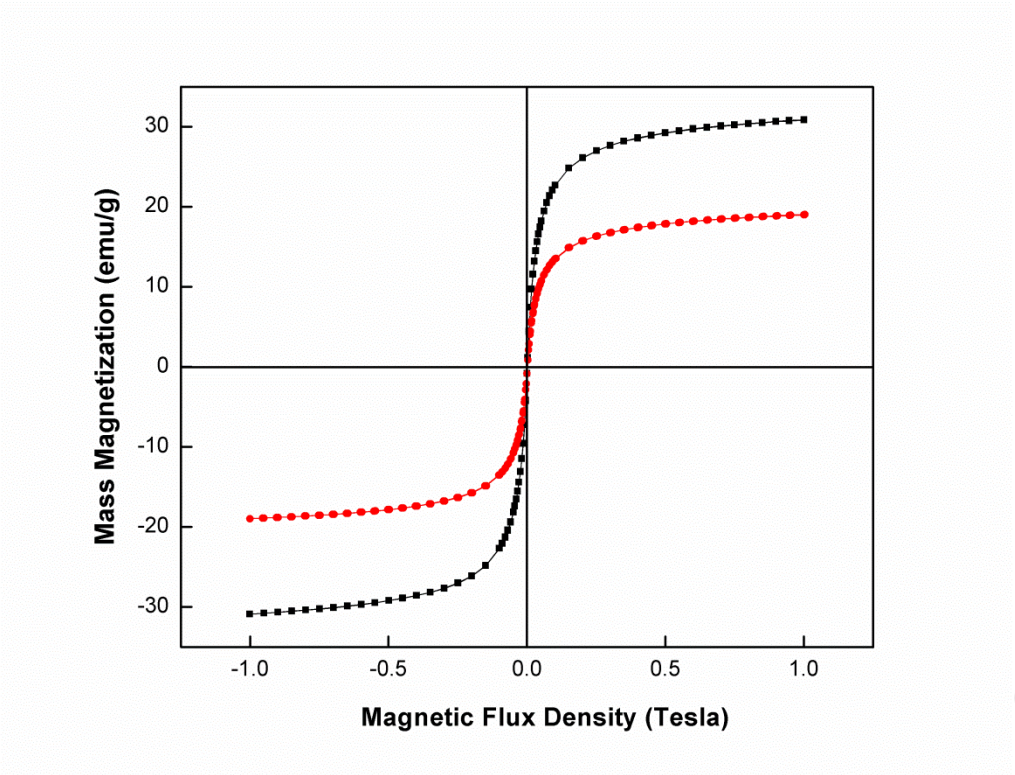

Figure 3.36 Mass magnetization vs magnetic flux density for bare iron oxide nanoparticles (black) and TA-coated iron oxide nanoparticles (red).

CHAPTER 4

CONCLUSION AND OUTLOOK

Iron oxide nanoparticles were synthesized by ultra-sonication based co-precipitation method. Multilayers of tannic acid and poly(2-isopropyl-2-oxazoline) were constructed on iron oxide nanoparticles via LbL technique at pH 4 through hydrogen bonding interactions. The highest number of layers that could be deposited onto iron oxide nanoparticles was found as 5. Further deposition of layers resulted in aggregation of LbL coated particles. Polymer molecular weight and concentration of polymer solutions were found to be highly critical on LbL coating of iron oxide nanoparticles.

An anti-cancer drug, doxorubicin (DOX) could be successfully loaded into LbL coated iron oxide nanoparticles at pH 7.5 and 25°C. The driving force for DOX loading was the electrostatic interaction among protonated amino groups of DOX and phenolate groups of TA at pH 7.5 as well as hydrogen bonding interactions among ether oxygens, carbonyl or hydroxyl groups of DOX and phenolic hydroxyl groups of TA. DOX could be released from the surface of LbL coated iron oxide nanoparticles via both pH and temperature trigger. For example, DOX could be released at pH 6 and 25°C due to protonation of phenolate groups and loss of electrostatic interactions among DOX and TA. DOX could also be released at 42.5°C when pH was kept constant at pH 7.5. The release at 42.5°C was correlated with LCST-type phase behavior of PIPOX. PIPOX transforms from extended to globular coil conformation above its LCST. This conformational transition led to formation of void-like structures within the multilayers and release of DOX from the surface. The increased kinetic energy of DOX molecules should also be another factor affecting the release of DOX from LbL coated iron oxide nanoparticles. DOX release was

found to be greatest at pH 6 and 42.5°C when DOX release was triggered via both pH and temperature.

Examination of magnetic properties of iron oxide nanoparticles via vibrating sample magnetometry (VSM) technique showed that iron oxide nanoparticles were superparamagnetic. Superparamagnetic property was retained even after coating the iron oxide nanoparticles with 1-layer of TA. However, saturation magnetization decreased from 32 to 20.2 after 1-layer of TA deposition onto iron oxide nanoparticles.

The work presented in this thesis developed strategies to coat iron oxide nanoparticles via LbL technique using hydrogen bonding polymers. Importantly, LbL coatings deposited onto iron oxide nanoparticles were both pH and temperature responsive. Iron oxide nanoparticles have wide range of applications especially in field of biomedicine as they are used as both carriers for targeted drug release and for imaging purpose. DOX loaded LbL coated iron oxide nanoparticles can be a promising materials for hyperthermia and magnetothermal release of functional molecules due to their superparamagnetic behavior and temperature response.

The future work on this study will comprise of the following parts:

- DOX loaded LbL coated iron oxide nanoparticles will be examined for magnetothermal trigger of DOX molecules. Particles will be exposed to alternating magnetic field with particular frequency. Heating iron oxide nanoparticles via alternating magnetic field is expected to result in an increase in the temperature of the polymer matrix which would induce the conformational transition of PIPOX chains and release of DOX molecules.

REFERENCES

[1] R.K. Iler, Multilayers of colloidal particles, J. Colloid Interface Sci. 21 (1966) 569–594.

[2] G. Decher, J. Schmitt, J.D. Hong, Buildup of ultrathin multilayer films by a self-assembly process : III . Consecutively alternating adsorption of anionic and cationic polyelectrolytes on charged surfaces, Thin Solid Films. 210–211 (1992) 831–835.

[3] W.B. Stockton, M.F. Rubner, Molecular-Level Processing of Conjugated Polymers. 4. Layer-by-Layer Manipulation of Polyaniline via Hydrogen-Bonding Interactions, Macromolecules. 30 (1997) 2717–2725.

[4] G. Decher, Fuzzy Nanoassemblies: Toward Layered Polymeric Multicomposites, Science (80-.). 277 (1997) 1232–1237.

[5] G.K. Such, A.P.R. Johnston, F. Caruso, Engineered hydrogen-bonded polymer multilayers: from assembly to biomedical applications, Chem. Soc. Rev. 40 (2011) 19–29.

[6] L. Wang, Z. Wang, X. Zhang, J. Shen, L. Chi, H. Fuchs, A new approach for the fabrication of an alternating multilayer film of poly(4-vinylpyridine) and poly(acrylic acid) based on hydrogen bonding, Macromol. Rapid Commun. 18 (1997) 509–514.

[7] S.A. Sukhishvili, S. Granick, Layered , Erasable Polymer Multilayers Formed by Hydrogen-Bonded Sequential Self-Assembly, Macromolecules. 35 (2002) 301–310.

[8] S.A. Sukhishvili, S. Granick, Layered, Erasable, Ultrathin Polymer Films, J. Am. Chem. Soc. 122 (2000) 9550–9551.

[9] N. Materials, ALtSTRQCT - The, 12 (1999) 789–796.

[10] M. Sato, M. Sano, van der Waals Layer-by-Layer Construction of a Carbon Nanotube 2D Network, (2005) 11490–11494.

[11] J. Chen, L. Huang, L. Ying, G. Luo, X. Zhao, Self-Assembly Ultrathin Films

Based on Diazoresins, Langmuir. 15 (1999) 7208–7212.

[12] G.K. Such, J.F. Quinn, A. Quinn, E. Tjipto, F. Caruso, Assembly of Ultrathin Polymer Multilayer Films by Click Chemistry, J. Am. Chem. Soc. 128 (2006) 9318–9319.

[13] Y. Shimazaki, M. Mitsuishi, S. Ito, M. Yamamoto, Preparation and Characterization of the Layer-by-Layer Deposited Ultrathin Film Based on the Charge-Transfer Interaction in Organic Solvents, Langmuir. 7463 (1998) 2768–2773.

[14] A. Rahim, H. Ejima, K.L. Cho, K. Kempe, M. Mu, J.P. Best, F. Caruso, Coordination-Driven Multistep Assembly of Metal − Polyphenol Films and Capsules, Chem. Mater. 26 (2014) 1645–1653.

[15] H. Hong, T.E. Mallouk, Electrochemical Measurements of Electron Transfer Rates through Zirconium 1,2-Ethanediylbis(phosphonate) Multilayer Films on Gold Electrodes, Langmuir. 7 (1991) 2362–2369.

[16] H. Lee, L.J. Kepley, H.G. Hong, T.E. Mallouk, Inorganic Analogues of Langmuir-Blodgett Films: Adsorption of Ordered Zirconium 1,10-Decanebisphosphonate Multilayers on Silicon Surfaces, J. Am. Chem. Soc. 110 (1988) 618–620.

[17] J.D. Hong, K. Lowack, J. Schmitt, G. Decher, J. Gutenberg-universit, Layer-by-layer deposited multilayer assemblies of polyelectrolytes and proteins : from ultrathin films to protein arrays, Prog. Colloid. Polym. Sci. 102 (1993) 98–102.

[18] S. Rauf, D. Zhou, C. Abell, D. Kang, Building three-dimensional nanostructures with active enzymes by surface templated layer-by-layer assembly {, Chem. Commun. 0 (2006) 1721–1723.

[19] M.M. De Villiers, D.P. Otto, S.J. Strydom, Y.M. Lvov, Introduction to nanocoatings produced by layer-by-layer (LbL) self-assembly, Adv. Drug Deliv. Rev. 63 (2011) 701–715.

[20] G. Decher, J.B. Schlenoff, Multilayer Thin Films: Sequential Assembly of Nanocomposite Materials, 2nd Edition, 2012.

[21] J.F. Quinn, A.P.R. Johnston, G.K. Such, A.N. Zelikin, F. Caruso, Next

generation, sequentially assembled ultrathin films: beyond electrostatics, Chem. Soc. Rev. 36 (2007) 707.

[22] G. Wu, X. Zhang, Layer-by-Layer Assembly: From Conventional to Unconventional Methods, Multilayer Thin Film. Seq. Assem. Nanocomposite Mater. Second Ed. 1 (2012) 43–67.

[23] P.K. Deshmukh, K.P. Ramani, S.S. Singh, A.R. Tekade, V.K. Chatap, G.B. Patil, S.B. Bari, Stimuli-sensitive layer-by-layer (LbL) self-assembly systems: Targeting and biosensory applications, J. Control. Release. 166 (2013) 294–306.

[24] P. Bertrand, A. Jonas, A. Laschewsky, R. Legras, Ultrathin polymer coatings by complexation of polyelectrolytes at interfaces: suitable materials, structure and properties, Macromol. Rapid Commun. 21 (2000) 319–348.

[25] G. Schneider, G. Decher, From Functional Core / Shell Nanoparticles Prepared via Layer-by-Layer Deposition to Empty Nanospheres, Nano Lett. 4 (2004) 1833–1839.

[26] N.A. Kotov, I. Dckiiny, J.H. Fendler, Layer-by-Layer Self-Assembly of Polyelectrolyte-Semiconductor Nanoparticle Composite Films, J. Phys. Chem. 99 (1995) 13069–13069.

[27] J.E. Wong, A.K. Gaharwar, D. Müller-Schulte, D. Bahadur, W. Richtering, Magnetic nanoparticle-polyelectrolyte interaction: a layered approach for biomedical applications., J. Nanosci. Nanotechnol. 8 (2008) 4033–4040. doi:

[28] T. Adalsteinsson, W.F. Dong, M. Schönhoff, Diffusion of 77 000 g/mol dextran in submicron polyelectrolyte capsule dispersions measured using PFG-NMR, J. Phys. Chem. B. 108 (2004) 20056–20063.

[29] F. Caruso, Nanoengineering of Inorganic and Hybrid Hollow Spheres by Colloidal Templating, Science (80-.). 282 (1998) 1111–1114.

[30] E. Donath, G.B. Sukhorukov, F. Caruso, S.A. Davis, H. Möhwald, Novel Hollow Polymer Shells by Colloid-Templated Assembly of Polyelectrolytes, Angew. Chemie Int. Ed. 37 (1998) 2201–2205.

[31] M. Delcea, H. Möhwald, A.G. Skirtach, Stimuli-responsive LbL capsules and nanoshells for drug delivery, Adv. Drug Deliv. Rev. 63 (2011) 730–747.

[32] M. Hrubý, S.K. Filippov, P. Štěpánek, Smart polymers in drug delivery

systems on crossroads: Which way deserves following?, Eur. Polym. J. 65 (2015)

[33] R. Ghizal, Smart Polymers and their Applications, Int. J. Eng. Technol. Manag. Appl. Sci. 2 (2014) 104–115.

[34] D. Schmaljohann, Thermo- and pH-responsive polymers in drug delivery, Adv. Drug Deliv. Rev. 58 (2006) 1655–1670.

[35] P. Bawa, V. Pillay, Y.E. Choonara, L.C. du Toit, Stimuli-responsive polymers and their applications in drug delivery, Biomed. Mater. 4 (2009) 1–15.

[36] S. Mura, J. Nicolas, P. Couvreur, Stimuli-responsive Nanocarriers for Drug Delivery, Nat. Mater. 12 (2013) 991–1003.

[37] E. Lim, T. Kim, S. Paik, S. Haam, Y. Huh, K. Lee, Nanomaterials for Theranostics : Recent Advances and Future Challenges, Chem. Reviwes. 115 (2015) 327–394.

[38] W. Tong, X. Song, C. Gao, Layer-by-layer assembly of microcapsules and their biomedical applications, Chem. Soc. Rev. 41 (2012) 6103.

[39] Y. Qiu, K. Park, Environment-sensitive hydrogels for drug delivery, Adv. Drug Deliv. Rev. 64 (2012) 49–60.

[40] K. Yoshida, T. Ono, Y. Kashiwagi, S. Takahashi, K. Sato, J. Anzai, pH-Dependent Release of Insulin from Layer-by-Layer-Deposited Polyelectrolyte Microcapsules, Polymers (Basel). 7 (2015) 1269–1278.

[41] E. Kharlampieva, S.A. Sukhishvili, Release of a dye from hydrogen-bonded and electrostatically assembled polymer films triggered by adsorption of a polyelectrolyte, Langmuir. 20 (2004) 9677–9685.

[42] G.B. Sukhorukov, A.A. Antipov, A. Voigt, E. Donath, H. M??hwald, pH-controlled macromolecule encapsulation in and release from polyelectrolyte multilayer nanocapsules, Macromol. Rapid Commun. 22 (2001) 44–46.

[43] X. Zhao, P. Liu, PH-sensitive fluorescent hepatocyte-targeting multilayer polyelectrolyte hollow microspheres as a smart drug delivery system, Mol. Pharm. 11 (2014) 1599–1610.

[44] G.F. Luo, X.D. Xu, J. Zhang, J. Yang, Y.H. Gong, Q. Lei, H.Z. Jia, C. Li, R.X. Zhuo, X.Z. Zhang, Encapsulation of an adamantane-doxorubicin prodrug

in pH-responsive polysaccharide capsules for controlled release, ACS Appl. Mater. Interfaces. 4 (2012) 5317–5324.

[45] D.X.Q. Liu, P.C. Picart, Layer-by-layer assemblies for cancer treatment and diagnosis, Adv. Mater. 28 (2016) 1295–1301.

[46] I. Erel, H.E. Karahan, C. Tuncer, V. Bütün, A.L. Demirel, Hydrogen-bonded multilayers of micelles of a dually responsive dicationic block copolymer, Soft Matter. 8 (2012) 827–836.

[47] S.R. Abulateefeh, S.G. Spain, J.W. Aylott, W.C. Chan, M.C. Garnett, C. Alexander, Thermoresponsive polymer colloids for drug delivery and cancer therapy, Macromol. Biosci. 11 (2011) 1722–1734.

[48] F. Eeckman, K. Amighi, A. ´ J. Moes, Effect of some physiological and non-physiological compounds on the phase transition temperature of thermoresponsive polymers intended for oral controlled-drug delivery, Int. J. Pharm. 222 (2001) 259–270.

[49] M. Ebara, Y. Kotsuchibashi, R. Narain, N. Idota, Y.-J. Kim, J.M. Hoffman, K. Uto, T. Aoyagi, Smart Biomaterials, 2014.

[50] E.S. polymers and their bioconjugatesok Gil, S.M. Hudson, Stimuli-reponsive polymers and their bioconjugates, Polym. Sci. 29 (2004) 1173–1222.

[51] E.A. Clark, J.E.G. Lipson, LCST and UCST behavior in polymer solutions and blends, Polymer (Guildf). 53 (2012) 536–545.

[52] E. Kharlampieva, V. Kozlovskaya, J. Tyutina, S.A. Sukhishvili, Hydrogen-bonded multilayers of thermoresponsive polymers, Macromolecules. 38 (2005) 10523–10531.

[53] D. Kuckling, A. Richter, K. Arndt, Temperature and pH-Dependent Swelling Behavior of Poly (N-isopropylacrylamide) Copolymer Hydrogels and Their Use in Flow Control, Macromol. Mater. Eng. 288 (2003) 144–151.

[54] V. Kozlovskaya, E. Kharlampieva, I. Drachuk, D. Cheng, V. V. Tsukruk, Responsive microcapsule reactors based on hydrogen-bonded tannic acid layer-by-layer assemblies, Soft Matter. 6 (2010) 3596.

[55] Z. Zhao, L. Yin, G. Yuan, L. Wang, Layer-by-layer assembly of two temperature-responsive homopolymers at neutral ph and the temperature-

dependent solubility of the multilayer film, Langmuir. 28 (2012) 2704–2709.

[56] C.J. Huang, F.C. Chang, Using click chemistry to fabricate ultrathin thermoresponsive microcapsules through direct covalent layer-by-layer assembly, Macromolecules. 42 (2009) 5155–5166.

[57] J.F. Quinn, F. Caruso, Facile Tailoring of Film Morphology and Release Properties Using Layer-by-Layer Assembly of Thermoresponsive Materials, Langmuir. 20 (2004) 20–22.

[58] M. Prevot, C. Déjugnat, H. Möhwald, G.B. Sukhorukov, Behavior of temperature-sensitive PNIPAM confined in polyelectrolyte capsules, ChemPhysChem. 7 (2006) 2497–2502.

[59] J.E. Wong, A.K. Gaharwar, D. Müller-Schulte, D. Bahadur, W. Richtering, Dual-stimuli responsive PNiPAM microgel achieved via layer-by-layer assembly: Magnetic and thermoresponsive, J. Colloid Interface Sci. 324 (2008) 47–54.

[60] M. Motornov, Y. Roiter, I. Tokarev, S. Minko, Stimuli-responsive nanoparticles, nanogels and capsules for integrated multifunctional intelligent systems, Prog. Polym. Sci. 35 (2010) 174–211.

[61] N. Adams, U.S. Schubert, Poly(2-oxazolines) in biological and biomedical application contexts, Adv. Drug Deliv. Rev. 59 (2007) 1504–1520.

[62] T.X. Viegas, M.D. Bentley, J.M. Harris, Z. Fang, K. Yoon, B. Dizman, R. Weimer, A. Mero, G. Pasut, F.M. Veronese, Polyoxazoline: Chemistry, properties, and applications in drug delivery, Bioconjug. Chem. 22 (2011) 976–986.

[63] R. Hoogenboom, Poly(2-oxazoline)s: A polymer class with numerous potential applications, Angew. Chemie - Int. Ed. 48 (2009) 7978–7994.

[64] I. Erel, H. Schlaad, A.L. Demirel, Effect of structural isomerism and polymer end group on the pH-stability of hydrogen-bonded multilayers, J. Colloid Interface Sci. 361 (2011) 477–482.

[65] M. Haktaniyan, S. Atilla, E. Cagli, I. Erel-Goktepe, pH- and Temperature-Induced Release of Doxorubicin from Multilayers of Poly(2-isopropyl-2-oxazoline) and Tannic Acid, Polym. Int. (2017) 36.

[66] A.B. da Fonseca Antunes, M. Dierendonck, G. Vancoillie, J.P. Remon, R. Hoogenboom, B.G. De Geest, Hydrogen bonded polymeric multilayer films assembled below and above the cloud point temperature, Chem. Commun. 49 (2013) 9663.

[67] A. Sundaramurthy, M. Vergaelen, S. Maji, R. Auzély-Velty, Z. Zhang, B.G. De Geest, R. Hoogenboom, Hydrogen Bonded Multilayer Films Based on Poly(2-oxazoline)s and Tannic Acid, Adv. Healthc. Mater. 3 (2014) 2040–2047.

[68] K. Kempe, S.L. Ng, K.F. Noi, M. Müllner, S.T. Gunawan, F. Caruso, Clickable poly(2-oxazoline) architectures for the fabrication of low-fouling polymer capsules, ACS Macro Lett. 2 (2013) 1069–1072.

[69] K. Kempe, S.L. Ng, S.T. Gunawan, K.F. Noi, F. Caruso, Intracellularly degradable hydrogen-bonded polymer capsules, Adv. Funct. Mater. 24 (2014) 6187–6194.

[70] S. Hendessi, P.T. Güner, A. Miko, A.L. Demirel, Hydrogen bonded multilayers of poly(2-ethyl-2-oxazoline) stabilized silver nanoparticles and tannic acid, Eur. Polym. J. 88 (2017) 666–678.

[71] S. Carregal-Romero, P. Guardia, X. Yu, R. Hartmann, T. Pellegrino, W.J. Parak, Magnetically triggered release of molecular cargo from iron oxide nanoparticle loaded microcapsules, Nanoscale. 7 (2015) 570–576.

[72] W. Wang, L. Liu, X.J. Ju, D. Zerrouki, R. Xie, L. Yang, L.Y. Chu, A novel thermo-induced self-bursting microcapsule with magnetictargeting property, ChemPhysChem. 10 (2009) 2405–2409.

[73] S.H. Hu, C.H. Tsai, C.F. Liao, D.M. Liu, S.Y. Chen, Controlled rupture of magnetic polyelectrolyte microcapsules for drug delivery, Langmuir. 24 (2008) 11811–11818.

[74] L.L. Lao, R. V. Ramanujan, Magnetic and hydrogel composite materials for hyperthermia applications, J. Mater. Sci. Mater. Med. 15 (2004) 1061–1064.

[75] D.H. Kim, D.E. Nikles, D.T. Johnson, C.S. Brazel, Heat generation of aqueously dispersed CoFe2O4 nanoparticles as heating agents for magnetically activated drug delivery and hyperthermia, J. Magn. Magn.

Mater. 320 (2008) 2390–2396.

[76] N. A. Peppas, Y. Huang, M. Torres-Lugo, J.H. Ward, J. Zhang, Physicochemical Foundations and Structural Design of Hydrogels in Medicine and Biology, Annu. Rev. Biomed. Eng. 2 (2002) 9–29.

[77] C.S. Brazel, Expert Review Magnetothermally-responsive Nanomaterials : Combining Magnetic Nanostructures and Thermally-Sensitive Polymers for Triggered Drug Release, Pharm. Res. 26 (2009) 644–656.

[78] S.R. Sershen, S.L. Westcott, N.J. Halas, J.L. West, Independent optically addressable nanoparticle-polymer optomechanical composites, Appl. Phys. Lett. 80 (2002) 4609–4611.

[79] S.L. Huang, Liposomes in ultrasonic drug and gene delivery, Adv. Drug Deliv. Rev. 60 (2008) 1167–1176.

[80] E.R. Edelman, J. Kost, H. Bobeck, R. Langer, Regulation of drug release from polymer matrices by oscillating magnetic fields, J. Biomed. Mater. Res. 19 (1985) 67–83.

[81] R. Hergt, W. Andrae, C.G. d'Ambly, I. Hilger, W.A. Kaiser, U. Richter, H.G. Schmidt, Physical limits of hyperthermia using magnetite fine particles, IEEE Trans. Magn. 34 (1998) 3745–3754.

[82] I. Ankareddi, M.L. Hampel, M.K. Sewell, D.-H. Kim, C.S. Brazel, Temperature controlled grafted polymer network incorporated with magnetic nano particles to control drug release induced by an external magnetothermal trigger, 2007 NSTI Nanotechnol. Conf. Trade Show - NSTI Nanotech 2007, Tech. Proc. 2 (2007) 431–434.

[83] C.S.S.R. Kumar, F. Mohammad, Magnetic nanomaterials for hyperthermia-based therapy and controlled drug delivery, Adv. Drug Deliv. Rev. 63 (2011) 789–808.

[84] M. Johannsen, B. Thiesen, P. Wust, A. Jordan, M. Johannsen, B. Thiesen, P. Wust, A. Jordan, M. Johannsen, B. Thiesen, P. Wust, A. Jordan, Magnetic nanoparticle hyperthermia for prostate cancer, Int. J. Hyperth. 26 (2010) 790–795.

[85] R.R. Baker, J.G. Mather, J.H. Kennaugh, Magnetic Bones in Human Sinuses,

Nature. 301 (1983) 78–80.

[86] N.A. Spladin, Magnetic Materials : Fundamentals and Applications, Second Edi, Cambridge University Press, 2011.

[87] B. Issa, I.M. Obaidat, B.A. Albiss, Y. Haik, Magnetic Nanoparticles : Surface Effects and Properties Related to Biomedicine Applications, Int. J. Mol. Sci. 14 (2013) 21266–21305.

[88] J. Yang, S.B. Park, H.G. Yoon, Y.M. Huh, S. Haam, Preparation of poly caprolactone nanoparticles containing magnetite for magnetic drug carrier, Int. J. Pharm. 324 (2006) 185–190.

[89] H. Wu, G. Liu, X. Wang, J. Zhang, Y. Chen, J. Shi, H. Yang, H. Hu, S. Yang, Solvothermal synthesis of cobalt ferrite nanoparticles loaded on multiwalled carbon nanotubes for magnetic resonance imaging and drug delivery, Acta Biomater. 7 (2011) 3496–3504.

[90] A.H. Lu, E.L. Salabas, F. Schüth, Magnetic nanoparticles: Synthesis, protection, functionalization, and application, Angew. Chemie - Int. Ed. 46 (2007) 1222–1244.

[91] Pankhurst, J. Connolly, S.K. Jones, D. J, Applications of magnetic nanoparticles in biomedicine, J. Phys. D …. 36 (2003) R167–R181.

[92] T. Indira, Magnetic Nanoparticles: A Review, Int. J. Pharm. 3 (2010) 1035–1042.

[93] A.S. Teja, P. Koh, Synthesis, properties, and applications of magnetic iron oxide nanoparticles, Prog. Cryst. Growth Charact. Mater. 55 (2009) 22–45.

[94] B.R. Dronskowski, The Little Maghemite Story : A Classic Functional Material, Adv. Funtional Mater. 11 (2001) 2000–2002.

[95] R.M. Cornell, U. Schwertmann, Iron Oxides in the Laboratory, 2000.

[96] C. Lin, K. Ho, Synthesis of superparamagnetic magnetite nanoparticles for thermoresponsive drug delivery, Nanotech. 2 (2007) 405–408.

[97] K. Woo, J. Hong, S. Choi, H. Lee, J. Ahn, C.S. Kim, S.W. Lee, Easy Synthesis and Magnetic Properties of Iron Oxide Nanoparticles, Chem. Mater. 16 (2004) 2814–2818.

[98] R. Massart, Preparation of aqueous magnetic liquids in alkaline and acidic

media, IEEE Trans. Magn. 17 (1981) 1247–1248.

[99] P.P. Wust, U. Gneveckow, P.P. Wust, M. Johannsen, D. Böhmer, T. Henkel, J. Sehouli, R. Felix, J. Ricke, A. Jordan, M. Johannsen, D. Böhmer, T. Henkel, F. Kahmann, J. Sehouli, R. Felix, J. Ricke, A. Jordan, A. Jordan, Magnetic nanoparticles for interstitial thermotherapy – feasibility , tolerance and achieved temperatures, Int. J. Hyperth. 22 (2006) 673–685.

[100] A.A. Cavallaro, M.N. MacGregor-Ramiasa, K. Vasilev, Antibiofouling Properties of Plasma-Deposited Oxazoline-Based Thin Films, ACS Appl. Mater. Interfaces. 8 (2016) 6354–6362.

[101] M. Mazur, A. Barras, V. Kuncser, A. Galatanu, V. Zaitzev, K. V. Turcheniuk, P. Woisel, J. Lyskawa, W. Laure, A. Siriwardena, R. Boukherrouba, S. Szunerits, Iron oxide magnetic nanoparticles with versatile surface functions based on dopamine anchors, Nanoscale. 5 (2013) 2692–2702.

[102] M. Mazur, A. Barras, V. Kuncser, A. Galatanu, V. Zaitzev, P. Woisel, J. Lyskawa, W. Laure, A. Siriwardena, R. Boukherroub, S. Szunerits, Iron Oxide Magnetic Nanoparticles with Versatile Surface Functions Based on Dopamine Anchors, Nanoscale. 5 (2013) 2692–2702.

[103] X. Huang, A. Schmucker, J. Dyke, S.M. Hall, J. Retrum, B. Stein, N. Remmes, D. V Baxter, B. Dragnea, L.M. Bronstein, Magnetic nanoparticles with functional silanes: evolution of well-defined shells from anhydride containing silane., J. Mater. Chem. 19 (2009) 4231–4239.

[104] A.B. Mikhaylova, V.P. Sirotinkin, M.A. Fedotov, V.P. Korneyev, B.F. Shamray, L. V. Kovalenko, Quantitative determination of content of magnetite and maghemite in their mixtures by X-ray diffraction methods, Inorg. Mater. Appl. Res. 7 (2016) 130–136.

[105] M. Shen, H. Cai, X. Wang, X. Cao, K. Li, S.H. Wang, R. Guo, L. Zheng, G. Zhang, X. Shi, Facile one-pot preparation, surface functionalization, and toxicity assay of APTS-coated iron oxide nanoparticles, Nanotechnology. 23 (2012) 105601.

[106] H. Qu, D. Caruntu, H. Liu, C.J. O'Connor, Water-dispersible iron oxide magnetic nanoparticles with versatile surface functionalities, Langmuir. 27

(2011) 2271–2278.

[107] S. Mahadevan, G. Gnanaprakash, J. Philip, B.P.C. Rao, T. Jayakumar, X-ray diffraction-based characterization of magnetite nanoparticles in presence of goethite and correlation with magnetic properties, Phys. E Low-Dimensional Syst. Nanostructures. 39 (2007) 20–25.

[108] V.A. Izumrudov, E. Kharlampieva, S.A. Sukhishvili, Multilayers of a globular protein and a weak polyacid: Role of polyacid ionization in growth and decomposition in salt solutions, Biomacromolecules. 6 (2005) 1782–1788.

[109] M. Bagtash, Y. Yamini, E. Tahmasebi, J. Zolgharnein, Z. Dalirnasab, Magnetite nanoparticles coated with tannic acid as a viable sorbent for solid-phase extraction of Cd^{2+}, Co^{2+} and Cr^{3+}, Microchim. Acta. 183 (2016) 449–456.

[110] S.Y. Yang, D. Lee, R.E. Cohen, M.F. Rubner, Bioinert solution-cross-linked hydrogen-bonded multilayers on colloidal particles, Langmuir. 20 (2004) 5978–5981.

[111] M.A. Pantoja-Castro, H. González-Rodríguez, Study by infrared spectroscopy and thermogravimetric analysis of Tannins and Tannic acid, Rev. Latinoam. Química. 39 (2012) 107–112.

[112] C. Sanson, C. Schatz, J.F. Le Meins, A. Soum, J. Thévenot, E. Garanger, S.S. Lecommandoux, A simple method to achieve high doxorubicin loading in biodegradable polymersomes, J. Control. Release. 147 (2010) 428–435.

[113] M. Mahmoudi, A. Simchi, A.S. Milani, P. Stroeve, Cell toxicity of superparamagnetic iron oxide nanoparticles, J. Colloid Interface Sci. 336 (2009) 510–518.

[114] M. Mikhaylova, D.K. Kim, N. Bobrysheva, M. Osmolowsky, V. Semenov, T. Tetal, T. Tsakalakos, M. Muhammed, Superparamagnetism of magnetite nanoparticles: dependence on surface modification, Langmuir. 20 (2004) 2472–2477.

APPENDIX A

CALIBRATION CURVES

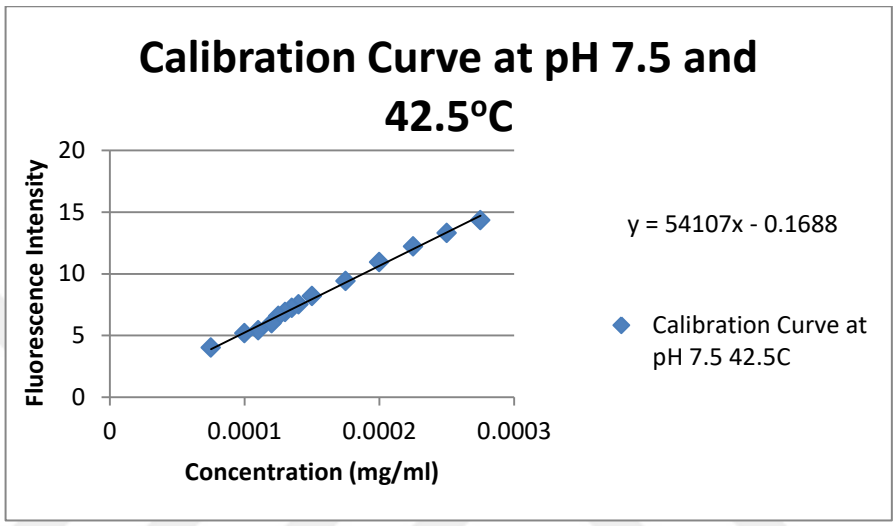

Figure A.1 Calibration curve of DOX solution at pH 7.5 and 42.5oC. Fluorescence intensity at 588 nm is plotted as a function of DOX concentration (mg/mL).

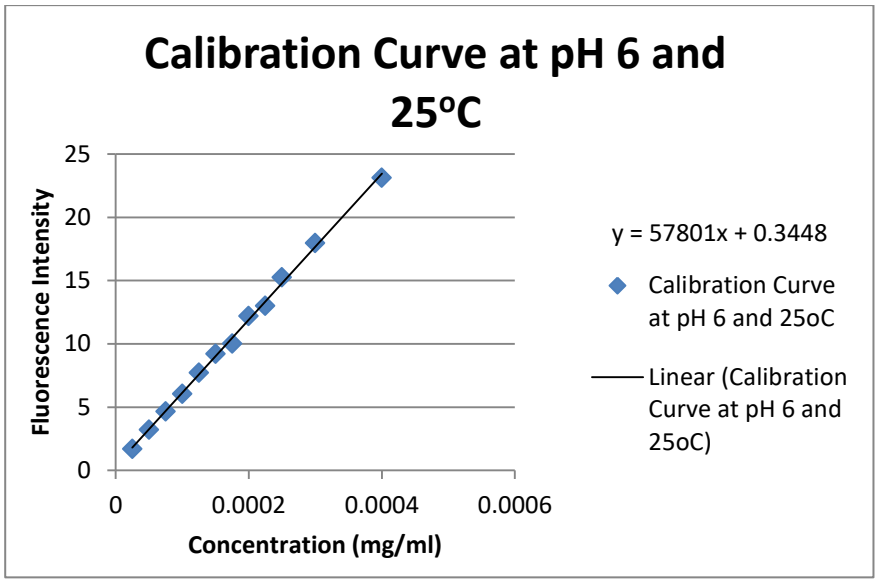

Figure A.2 Calibration curve of DOX solution at pH 6 and 25oC. Fluorescence intensity at 588 nm is plotted as a function of DOX concentration (mg/mL).

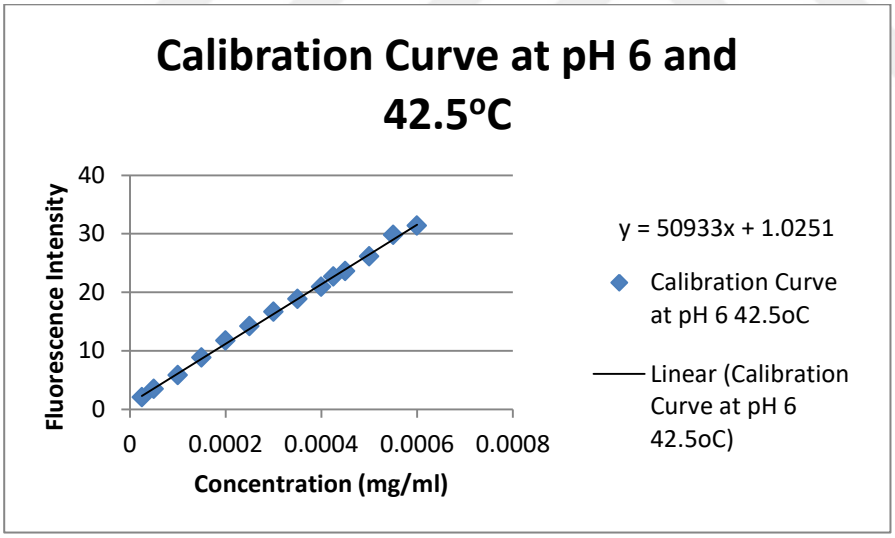

Figure A.3 Calibration curve of DOX solution at pH 6 and 42.5oC. Fluorescence intensity at 588 nm is plotted as a function of DOX concentration (mg/mL).